

Spinor helicity methods in high-energy factorization: efficient momentum-space calculations in the Color Glass Condensate formalism

Alejandro Ayala^{1,2}, Martin Hentschinski^{1,3}, Jamal Jalilian-Marian^{4,5,6},
Maria Elena Tejeda-Yeomans⁷

¹Instituto de Ciencias Nucleares, Universidad Nacional Autónoma de México,
Apartado Postal 70-543, Ciudad de México 04510, Mexico

²Centre for Theoretical and Mathematical Physics, and Department of Physics,
University of Cape Town, Rondebosch 7700, South Africa

³Departamento de Acturía, Física y Matemáticas, Universidad de las Americas - Puebla
Santa Catarina Martir, 72820, Puebla, Mexico

⁴Department of Natural Sciences, Baruch College, CUNY,
17 Lexington Avenue, New York, NY 10010, USA

⁵CUNY Graduate Center, 365 Fifth Avenue, New York, NY 10016, USA

⁶Centre de Physique Théorique, École Polytechnique, CNRS,
Université Paris-Saclay, 91128 Palaiseau, France

⁷Departamento de Física, Universidad de Sonora, Boulevard Luis Encinas J. y Rosales,
Colonia Centro, Hermosillo, Sonora 83000, Mexico

March 6, 2024

Abstract

We use the spinor helicity formalism to calculate the cross section for production of three partons of a given polarization in Deep Inelastic Scattering (DIS) off proton and nucleus targets at small Bjorken x . The target proton or nucleus is treated as a classical color field (shock wave) from which the produced partons scatter multiple times. We reported our result for the final expression for the production cross section and studied the azimuthal angular correlations of the produced partons in [1]. Here we provide the full details of the calculation of the production cross section using the spinor helicity methods.

1 Introduction

The Color Glass Condensate (CGC) formalism (see [2] for a review) is an effective field theory approach to QCD at small x where the gluon density in a proton or nucleus is expected to be so large that the standard QCD-improved parton model must break down. In this limit it is more appropriate to treat the hadron or nucleus as a coherent color field rather than a collection of incoherent and individual partons. At the classical level, the CGC generalizes scattering via exchange of a single gluon to multiple gluon exchanges (high energy factorization). By including quantum loop effects, it resums the large logs of Bjorken x [3] (or

equivalently energy) as opposed to the leading twist collinear factorization formalism which resums large logs of the hard scale Q^2 . The Color Glass Condensate formalism is the appropriate one to use in the kinematic limit where $\log 1/x \gg \log Q^2$. This is typically the case for particle production in the low to intermediate p_t regime and in the forward rapidity region [4] where one probes the small x components of the target wave function.

The Color Glass Condensate formalism has been applied to various high energy processes. A first class of observables is associated with the forward hadron production at RHIC and the LHC (see [5] for a compilation of LHC forward physics observables and [6] for a compilation of the CGC-motivated phenomenology of particle production). While there are strong hints for the presence of gluon saturation effects in the observed suppression of forward hadron production cross section at RHIC and the LHC [7], the effect is far from being universally accepted as coming only from saturation. Models which modify the parton distribution functions of nuclei and add energy loss effects have also been used to fit the data [8]. Azimuthal angular correlations of produced di-hadrons have also been measured (in deuteron-gold collisions) and show a strong decorrelation of the azimuthal angle between the two produced hadrons in the forward rapidity region as predicted in the CGC formalism [9]. The away side peak is observed to be broader which can be understood to be due to multiple scattering. Furthermore, the magnitude of the peak is reduced which is due to the small x evolution of the target wave function which causes “nuclear shadowing”. Various angular correlations have also been suggested as possible probes of gluon saturation in the target [10, 11]. They all exhibit the same qualitative features in the CGC formalism which will be further probed by the current experiments at the LHC and in the proposed Electron-Ion Collider [12].

While much can be learned from hadron-hadron collisions, observables generally suffer from contaminations due to soft and collinear radiation. A much cleaner environment – both experimentally and theoretically – is, on the other hand, provided by photon induced processes. While much has been learned from the study of proton structure functions measured at the HERA experiment, ultra-peripheral collisions (UPCs) of protons on protons and nuclei on protons at the LHC, allow to study the currently most energetic photon-proton collisions, where either a large nucleus or a proton serve as the photon source. Among the most prominent observables explored so far is exclusive photo-production process of vector mesons such as the J/Ψ [13, 14]. Such processes are of particular interest since they allow to probe the gluon distribution in the proton down to very small values of Bjorken $x \sim 10^{-5}$, see [15] for CGC-related studies. While such CGC studies provide an excellent description of the energy dependence of the exclusive J/Ψ photo-production cross-section, the same energy dependence has also an excellent description in terms of (dilute) next-to-leading order BFKL evolution (see *e.g.* [16]) which, unlike the CGC-formalism, does not include corrections due to high densities. From a theoretical point of view the difficulty to distinguish low x evolution without (BFKL) and with (BK, JIMWLK) is related to the type of correlators probed by such observables: both proton structure functions and the amplitude for exclusive photo-production of vector mesons are directly proportional to the two-point correlator of two Wilson lines, which itself can be related to an unintegrated gluon density. The description of such observables is therefore at first identical for low (BFKL) and high (BK, JIMWLK) densities and the presence of high density effects only manifests itself through the particular form of low x evolution. Finding definite evidence for saturation effects requires therefore

evolution of the observables far into the low x region, well beyond the kinematical reach of current collider experiments.

In [1] we proposed triple jet/hadron production in DIS as an excellent probe of gluon saturation dynamics in a hadron or nucleus. Unlike the observables discussed above, the theoretical description of observables with multiple final states involves higher order correlators of Wilson lines in the target. As a consequence high density effects manifest themselves directly at the level of the observable without the need to invoke low x evolution. In particular there are substantial differences between a BFKL/low density and a CGC/high density description. While the measurement of such high multiplicity final states is much more cumbersome experimentally, such observables provide important complementary information to inclusive observables, and therefore allow to pin down the valid description of perturbative QCD in the low x region. The case of three jet/hadron production is then of particular interest, since such an observable provides two relative angles rather than one in the case of two-particle correlations, so there is an additional knob to turn. Furthermore there are two away side peaks, each of which will sensitively depend on saturation dynamics and small x evolution. We showed our final expression for the triple differential cross section in [1] and used it to study, quantitatively, the angular dependence of the cross section in certain kinematics. The present paper is dedicated to a presentation of the full details of the calculation, employing spinor helicity formalism (for introductory reviews see [17]) which leads to a major simplification of the calculation. For another recent application of the spinor helicity formalism in the framework of light-cone wave function see [18]; for a related calculation of 3 parton impact factor in DIS in the shock wave framework see also [19, 20]; see also the calculation of next-to-leading corrections to inclusive DIS of [21, 22].

This paper is organized in the following way: we write down the formal expressions for the production amplitude in Section 2 and proceed to study the space-time structure of the diagrams in Section 2.1 and 2.2. Various cuts of the diagrams are considered and shown to lead to vanishing of some diagrams due to the “wrong cut”. This allows us to re-write the expressions for the amplitude in a more compact way. We then give an overview of the spinor helicity formalism in Section 3 and proceed to apply it to the process considered. Major simplifications occur when one considers scattering and production of partons of a fixed helicity due to helicity conservation. We summarize in Section 4 and, using crossing symmetry, point out the connections between our results and Multi-Parton Scattering (MPI) in the projectile, in photon-jet or photon production in forward rapidity proton-nucleus collisions.

2 CGC amplitudes in momentum space

We consider production of three partons in DIS as depicted in Fig. 1,

$$\gamma^*(l) + \text{target}(P) \rightarrow q(p) + \bar{q}(q) + g(k) + X, \quad (1)$$

where the target can be a proton or nucleus and where $Q^2 = -l^2$ denotes the virtuality of the photon. We will study the process in the limit of high center of mass energy $\sqrt{s} \rightarrow \infty$ with $s = (l+P)^2$. To this end it is convenient to introduce light-cone vectors n, \bar{n} which are defined through the four momenta of virtual photon and target. With the Sudakov decomposition of

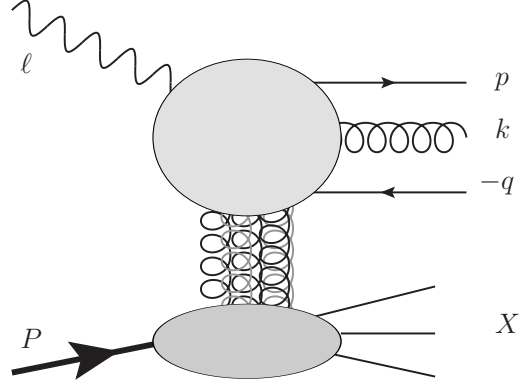


Figure 1:

a general four vector v given by

$$\begin{aligned} v_\mu &= v^+ \bar{n}_\mu + v^- n_\mu + v_t, & \text{where} & & n \cdot \bar{n} &= 1, & n^2 &= 0 = \bar{n}^2, \\ v^+ &= n \cdot v, & v^- &= \bar{n} \cdot v, & \text{and} & & v_t^2 &= -\mathbf{v}^2, \end{aligned} \quad (2)$$

we obtain for the momenta of initial particles

$$P_\mu = P^- n_\mu, \quad l_\mu = l^+ \bar{n} - \frac{Q^2}{l^+} n. \quad (3)$$

To include the possibility of arbitrary large gluon densities in the target, we represent the latter by its gluonic field which can reach a maximum strength of $A_\mu \sim 1/g$, with g the gauge coupling. To calculate scattering amplitudes in the high energy limit it is then convenient to treat the gluon field of the target as a background field (shock-wave); in light-cone gauge $A \cdot n = 0$, the only non-zero component is $A^-(x^+, x_t) = \delta(x^+) \alpha(x_t)$, while $A_t = 0$ in the high energy limit. Amplitudes are written in terms of momentum space quark and gluon propagators in the presence of the background field, see *e.g.* [23],

$$\begin{aligned} S_{F,il}(p, q) &\equiv S_{F,il}^{(0)}(p) (2\pi)^4 \delta^{(4)}(p - q) + S_{F,ij}^{(0)}(p) \cdot \tau_{F,jk}(p, q) \cdot S_{F,kl}^{(0)}(q), \\ G_{\mu\nu}^{ad}(p, q) &\equiv G_{\mu\nu}^{(0),ab}(p) (2\pi)^4 \delta^{(4)}(p - q) + G_{\mu\lambda}^{(0),ab}(p) \cdot \tau_G^{bc}(p, q) \cdot G_{\nu}^{(0),cd,\lambda}(q), \end{aligned} \quad (4)$$

which are directly obtained from Fourier transforming their corresponding counter parts in configuration space. In the above we use the conventional free fermion and gluon propagator,

$$S_{F,ij}^{(0)}(p) = \frac{i\delta_{ij}}{(\not{p} + i\epsilon)} \quad \text{and} \quad G_{\mu\nu}^{(0),ab} = \frac{i\delta^{ab} d_{\mu\nu}(k)}{(k^2 + i\epsilon)} \quad (5)$$

where

$$d_{\mu\nu}(k) = -g_{\mu\nu} + \frac{k_\mu n_\nu + k_\nu n_\mu}{n \cdot k} \quad (6)$$

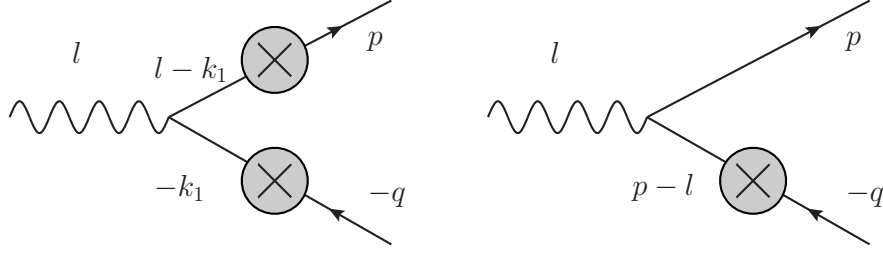


Figure 2: Left: Tree diagram with 2 insertions of the vertices Eqs. (7) and (8): the internal momentum k_1 is integrated over like a loop momenta i.e. with $\int d^4 k_1 / (2\pi)^4$. Right: Tree diagram with 1 insertion the vertices Eqs. (7) and (8): all momenta are fixed by external momenta

denotes the polarization tensor in the light-cone gauge, and

$$\begin{aligned}
 \begin{array}{c} p \\ \rightarrow \end{array} \text{---} \text{---} \text{---} \begin{array}{c} \text{X} \\ \text{---} \end{array} \begin{array}{c} \text{---} \\ \rightarrow \end{array} q &= \tau_{F,ij}(p, q) = 2\pi\delta(p^+ - q^+) \not{p} \\
 &\times \int d^2 z e^{iz \cdot (p-q)} \left\{ \theta(p^+) [V_{ij}(z) - 1_{ij}] - \theta(-p^+) [V_{ij}^\dagger(z) - 1_{ij}] \right\} \quad (7)
 \end{aligned}$$

$$\begin{aligned}
 \begin{array}{c} p \\ \rightarrow \end{array} \text{---} \text{---} \text{---} \begin{array}{c} \text{X} \\ \text{---} \end{array} \begin{array}{c} \text{---} \\ \rightarrow \end{array} q &= \tau_G^{ab}(p, q) = 2\pi\delta(p^+ - q^+) (-2p^+) \\
 &\times \int d^2 z e^{iz \cdot (p-q)} \left\{ \theta(p^+) [U^{ab}(z) - 1] - \theta(-p^+) [(U^{ab})^\dagger(z) - 1] \right\} \quad (8)
 \end{aligned}$$

with Wilson lines in fundamental (V) and adjoint (U) representation. They read

$$\begin{aligned}
 V(z) \equiv V_{ij}(z) &\equiv \text{P exp } ig \int_{-\infty}^{\infty} dx^+ A^{-,c}(x^+, z) t^c \\
 U(z) \equiv U^{ab}(z) &\equiv \text{P exp } ig \int_{-\infty}^{\infty} dx^+ A^{-,c}(x^+, z) T^c \quad (9)
 \end{aligned}$$

with $-iT_{ab}^c = f^{acb}$. To construct amplitudes in the presence of a (strong) background field, it is convenient to extend conventional QCD momentum space Feynman rules by two additional rules: (a) adding the vertices Eqs. (7) and (8) and (b) the requirement that all internal momenta p , i.e. momenta which cannot be expressed in terms of momenta of external particles, are integrated over with the measure $\int \frac{d^4 p}{(2\pi)^4}$, in 1-1 correspondence to conventional loop momenta. In tree diagrams such internal momenta arise if $n \geq 2$ vertices from Eqs. (7) and (8), are inserted into a single Feynman diagram; see Fig. 2 for an illustrative example. If the number n of produced colored particles in the final state is small, $n \leq 2$, the above method provides an efficient alternative to the calculation of matrix elements in the presence of large gluon densities, see [11, 24] for earlier examples. For final states with large multiplicities, $n \geq 3$, the method becomes inefficient due to the large number of Feynman diagrams which need to be considered. While the process $\gamma^* + \text{target} \rightarrow q + \bar{q}$ requires 3 diagrams, one finds

already 16 diagrams for the process $\gamma^* + \text{target} \rightarrow q + \bar{q} + g$. Moreover, calculations based on configuration space propagators suggest a large redundancy in the result, leading to large cancellations among different diagrams, which further complicate the use of momentum space methods. In the following we demonstrate that there is a direct way to use the emerging simplicity of the configuration space amplitudes for calculations in momentum space.

2.1 Cut diagrams according to negative and positive x^+

To achieve the required reduction of Feynman diagrams it is necessary to exploit the restriction of the interaction between projectile and target to the light-cone time-slice $x^+ = 0$, $A^-(z) \sim \delta(z^+)$. Such properties are naturally revealed in the configuration space and/or light-front formalism, which is the main reason for their preferred use over momentum space techniques. To make these properties and the associated reduction of diagrams explicit in momentum space, it is sufficient to associate with each propagator a separate minus-momentum variable. This can be achieved by introducing at each (standard QCD) vertex (where minus-momenta are conserved *i.e.*, excluding the vertices in Eqs. (7) and (8)), a delta function $\delta(\{p_{\text{in}}^-\} - \{p_{\text{out}}^-\})$, together with a corresponding integration over the newly introduced minus momentum variable; here $\{p_{\text{in}}^-\}$ ($\{p_{\text{out}}^-\}$) denotes the full set of incoming (outgoing) momenta of the vertex. Expressing each of these delta functions as a Fourier integral,

$$\delta(\{p_{\text{in}}^-\} - \{p_{\text{out}}^-\}) = \int \frac{dx^+}{2\pi} e^{-ix^+ \cdot (\{p_{\text{in}}^-\} - \{p_{\text{out}}^-\})}, \quad (10)$$

we finally obtain for each (standard QCD) vertex an integral over x_i^+ , $i = 1, \dots, N$ with N the total number of (standard QCD) vertices. These vertices are then connected by momentum space propagators which are Fourier transformed w.r.t. their plus momentum¹. At the vertices defined in Eqs. (7), (8) the minus momentum is not conserved and therefore no integration over minus coordinates appears; instead these vertices are associated with the ‘light-cone time’ $x^+ = 0$, *i.e.* we use $e^{ix^+ p^-} \Big|_{x^+=0} = 1$. Fourier transforming quark and gluon propagators w.r.t. to their plus momenta one finds easily the well known expressions

$$\begin{aligned} \tilde{S}_{F,kl}(x_{ij}^+; p^+, \mathbf{p}) &= \int \frac{dp^-}{2\pi} e^{-ip^- x_{ij}^+} S_{F,kl}(p) = \\ &= \delta_{kl} \frac{e^{-ip^- x_{ij}^+}}{2p^+} \left[\left(\theta(p^+) \theta(x_{ij}^+) + \theta(-p^+) \theta(-x_{ij}^+) \right) (\not{p} + m) + \delta(x_{ij}^+) \not{p} \right]_{p^- = \frac{p^2 + m^2}{2p^+}} \\ \tilde{G}_{\mu\nu}^{(0),ab}(x_{ij}^+; p^+, \mathbf{p}) &= \int \frac{dp^-}{2\pi} e^{-ip^- x_{ij}^+} G_{\mu\nu}^{(0),ab}(p) = \\ &= \delta_{ab} \frac{e^{-ip^- x_{ij}^+}}{2p^+} \left[\left(\theta(p^+) \theta(x_{ij}^+) + \theta(-p^+) \theta(-x_{ij}^+) \right) \cdot d_{\mu\nu}(p) + 2\delta(x_{ij}^+) \frac{n_\mu n_\nu}{p \cdot n} \right]_{p^- = \frac{p^2 + m^2}{2p^+}}. \quad (11) \end{aligned}$$

Here $x_{ij}^+ \equiv x_i^+ - x_j^+$. Using such propagators together with integrations over light-cone times x_i^+ at each vertex one re-obtains directly the light-cone time ordered Feynman rules of light-front perturbation theory (old-fashioned perturbation theory), see *e.g.* [22] which contains

¹The procedure is in 1-to-1 correspondence to the usual translation momentum space \leftrightarrow configuration space, while in the current setup we limit ourselves to the minus momenta/plus coordinates

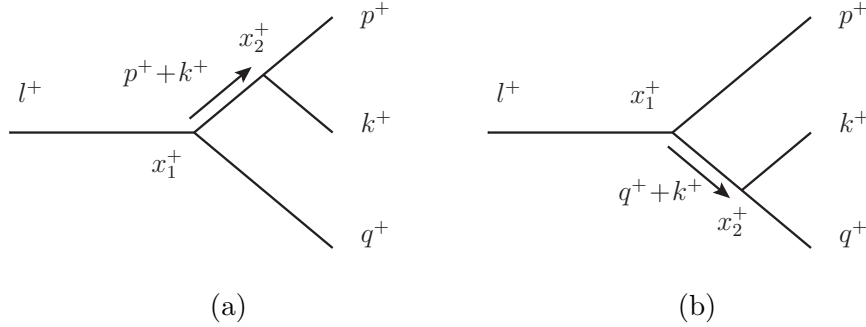


Figure 3: *Real corrections.* We have $l^+, p^+, q^+, k^+ > 0$ and $l^+ = p^+ + k^+ + q^+$

a recent and compact overview. In particular we find that it is natural to organize QCD interaction vertices into vertices before ($x_i^+ < 0$) and after the interaction ($x_i^+ > 0$) with the target field. In a nut-shell this result will allow us to evaluate to zero configurations which are absent in the light-front formalism for momentum space diagrams, simplifying enormously the reduction of diagrams at earlier stages of the calculation.

To be more precise, we first note that potential contact terms in the quark ($\sim \delta(x_{ij}^+) \not{n}$) and gluon ($\sim \delta(x_{ij}^+) n_\mu n_\nu$) propagators are absent, if the propagators connect with the vertices Eqs. (7) and (8): for the quark due to the identity $\not{n} \not{n} = 0$, for the gluon since $d_{\mu\nu}(p) \cdot n^\nu = 0$ and $n^2 = 0$ (if the vertex connects to a virtual gluon) and $\epsilon^{(\lambda)}(p)_\nu \cdot n^\nu = 0$ (if the vertex connects to a real gluon). Due to the absence of such contact terms it will be sufficient to limit the discussion to scalar skeleton diagrams, independent of the precise nature of particles. We further note that plus momenta are conserved at all vertices (including Eqs. (7) and (8)). On the other hand, since plus coordinates and plus momenta are the only components which receive special constraints from the propagators in the representation of Eq. (11), it is sufficient to study only their effect. The resulting diagrams are depicted in Fig. 3, where for the time being we ignore the presence of potential target interaction vertices Eqs. (7) and (8). In a next step we divide all integrals over light-cone times x_i^+ into a positive $x_i^+ > 0$ and a negative $x_i^+ < 0$ sector. While this is motivated by the restriction of the target interaction vertices to light-cone time $x_i^+ = 0$, this is irrelevant for the following reason. Using now that propagation from a vertex with negative light-cone time $x_j^+ < 0$ to a positive light-cone time $x_i^+ > 0$ implies $x_{ij}^+ > 0$ and therefore positive light-cone momentum $p^+ > 0$ (due to the structure of theta-functions in Eq. (11)), it is straight forward to verify that each skeleton diagram can be organized according to three possible “s-channel” cuts, see Fig. 4. It is easily possible to extend our result to the case of n final state particles: crossing from negative to positive light-cone times requires positive light-cone momentum and – vice versa – crossing from positive to negative light-cone times requires negative light-cone momentum. In the case of a tree skeleton diagram, all light-cone momenta are always positive and therefore crossing from positive to negative light-cone times is impossible. Moreover, once a certain line crosses from the negative to the positive light-cone time sector, all its daughter lines, *i.e.*, lines emerging from a splitting of this line, will have positive light-cone times by default. The resulting picture tells us that each individual diagram is characterized by all possible

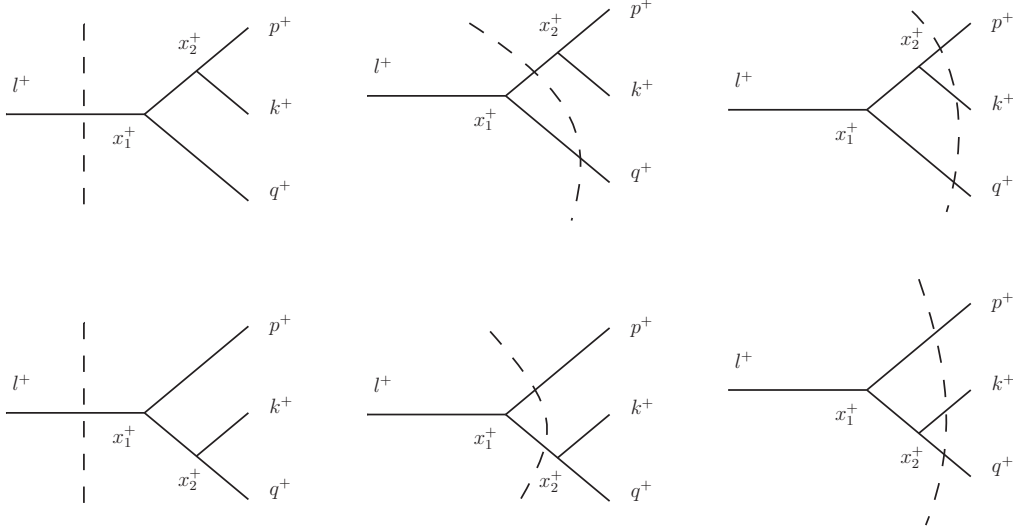


Figure 4: *Real corrections. The dashed line indicates the $x^+ = 0$ time-slice where the interaction with the target can take place. In addition there are also non-interacting contributions*

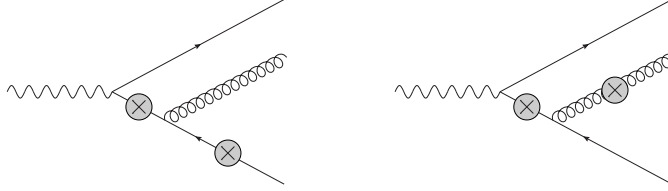


Figure 5: *Diagrams with interaction not aligned along a vertical cut and which gives therefore a zero contribution*

vertical lines through the diagrams (‘s-channel’ cuts) which indicate transition from negative to positive light-cone time.

The benefit of this result for the study of the interaction with the target field should be apparent by now: since vertices, Eqs. (7) and (8), are limited to light-cone time $x_i^+ = 0$, such vertices can only be inserted in a “cut” line. Insertions in un-cut lines, are immediately zero, see Fig. 5 for two configurations which cannot occur. Note that this result applies separately for each individual Feynman diagram and holds regardless of whether the actual evaluation takes place in configuration, momentum or mixed *i.e.* light-front space. While this leads already to a significant reduction in the number of Feynman diagrams to be evaluated, the remaining set of diagrams still contains a sizable fraction of redundant contributions. In particular there are large cancellations between diagrams where we place a target interaction vertex Eqs. (7), (8) at the $z_i^+ = 0$ cut and diagrams where such interaction is absent, see Fig. 6 for an example.

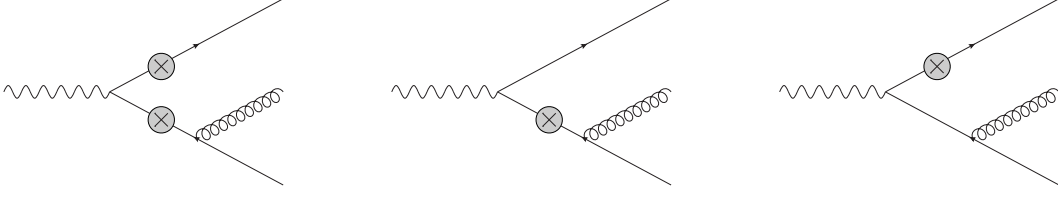


Figure 6: *Diagrams with and without interaction which belong to the same cut.*

2.2 Further reduction of diagrams

To reduce the number of diagrams further, it is necessary to study the Fourier transform of the complete propagators (containing both interacting and non-interacting) parts, Eq. (4). Using these propagators for all lines in diagrams (for external lines this implies the use of the LSZ-reduction procedure, see *e.g.* [11]) the full process can be represented in terms of two diagrams only. On the level of scalar skeleton graphs these are precisely those of Fig. 3. It is well known that such complete propagators can be written in configuration space in three parts: one term is associated with crossing from negative to positive light-cone time x^+ and is directly proportional to either a Wilson line (positive light-cone momentum fraction) or a hermitian conjugate Wilson line (negative light-cone momentum fraction). The other two terms describe free propagation between two points with either negative or positive light-cone time. For the following discussion the following form is sufficient:

$$\begin{aligned}
& \int \frac{dp^-}{2\pi} \int \frac{dq^-}{2\pi} e^{-ip^-x^+} e^{iq^-y^+} \left[S_{F,il}^{(0)}(p) (2\pi)^4 \delta^{(4)}(p-q) + S_{F,ij}^{(0)}(p) \cdot \tau_{F,jk}(p,q) \cdot S_{kl}^{(0)}(q) \right] \\
&= (2\pi)^3 \delta(p^+ - q^+) \delta^{(2)}(p_t - q_t) \tilde{S}_{F,il}^{(0)}(x^+ - y^+; p^+, p_t) \theta(x^+ \cdot y^+) \\
&\quad + \tilde{S}_{F,il}^{(V,V^\dagger)}(x^+, y^+; p^+, p_t; q^+, q_t) \\
& \int \frac{dp^-}{2\pi} \int \frac{dq^-}{2\pi} e^{-ip^-x^+} e^{iq^-y^+} \left[G_{\mu\nu}^{(0),ab}(p) (2\pi)^4 \delta^{(4)}(p-q) + G_{\mu\alpha}^{(0),ac}(p) \cdot \tau_G^{cd}(p,q) \cdot G_{\alpha\nu}^{(0),db}(q) \right] \\
&= (2\pi)^3 \delta(p^+ - q^+) \delta^{(2)}(p_t - q_t) \tilde{G}_{\mu\nu}^{(0),ab}(x^+ - y^+; p^+, p_t) \theta(x^+ \cdot y^+) \\
&\quad + \tilde{G}_{\mu\nu}^{ab,(U,U^\dagger)}(x^+, y^+; p^+, p_t; q^+, q_t) \quad (12)
\end{aligned}$$

where $\tilde{S}_{F,il}^{(0)}$, $\tilde{G}_{\mu\nu}^{(0),ab}$ are given by Eq. (11). The second term necessarily involves crossing the slice $x^+ = 0$ and is given by

$$\begin{aligned}
& \tilde{S}_{F,il}^{(V,V^\dagger)}(x^+, y^+; p^+, p_t; q^+, q_t) \\
&= \theta(p^+) \tilde{S}_{F,ij}(x^+, p^+, p_t) \not{n} \tilde{S}_{F,kl}(-y^+; p^+, q_t) \cdot 2\pi \delta(p^+ - q^+) \int d^2 z_t e^{iz_t \cdot (p_t - q_t)} V_{jk}(z_t) \\
&\quad - \theta(-p^+) \tilde{S}_{F,ij}(x^+, p^+, p_t) \not{n} \tilde{S}_{F,kl}(-y^+; p^+, q_t) \cdot 2\pi \delta(p^+ - q^+) \int d^2 z_t e^{iz_t \cdot (p_t - q_t)} V_{jk}^\dagger(z_t) \\
&= \tilde{S}_{F,ij}(x^+, p^+, p_t) \cdot \bar{\tau}_{F,jk}(p, q) \cdot \tilde{S}_{F,kl}(-y^+; p^+, q_t) \quad (13)
\end{aligned}$$

where the condition $p^+ > 0$ ($p^+ < 0$) selects automatically the configuration $x^+ > 0 > y^+$ ($x^+ < 0 < y^+$). Similarly one has in the case of gluons

$$\tilde{G}_{\mu\nu}^{ab,(U,U^\dagger)}(x^+, y^+; p^+, p_t; q^+, q_t) = \tilde{G}_{\mu\alpha}^{(0),ac}(x^+, p^+, p_t) \bar{\tau}_G^{cd}(p, q) \tilde{G}_{\alpha\nu}^{(0),db}(-y^+; p^+, q_t) \quad (14)$$

where we defined

$$\begin{aligned}
\text{Diagram 1: } & \text{A horizontal line with momentum } p \text{ entering from the left and momentum } q \text{ exiting to the right. In the middle, there is a black diamond vertex.} \\
& = \bar{\tau}_{F,ij}(p, q) = 2\pi\delta(p^+ - q^+) \cdot \not{p} \\
& \cdot \int d^2z e^{iz \cdot (p-q)} \left\{ \theta(p^+) V_{ij}(z) - \theta(-p^+) V_{ij}^\dagger(z) \right\} \quad (15)
\end{aligned}$$

$$\begin{aligned}
\text{Diagram 2: } & \text{A horizontal line with momentum } p \text{ entering from the left and momentum } q \text{ exiting to the right. In the middle, there is a black diamond vertex with four curly loops attached to it.} \\
& = \bar{\tau}_G^{ab}(p, q) = 2\pi\delta(p^+ - q^+) \cdot (-2p^+) \\
& \cdot \int d^2z e^{iz \cdot (p-q)} \left\{ \theta(p^+) U^{ab}(z) - \theta(-p^+) (U^{ab})^\dagger(z) \right\} \quad (16)
\end{aligned}$$

Applying now these results to the (skeleton) diagrams, Fig. 4, we now find that each “cut” line must necessarily come with a vertex, Eqs. (15) and (16). The “un-cut” lines can only come with a free propagator. At first these propagators are limited to positive or negative light-cone time only and therefore cannot be directly related to their momentum space counter-parts. Due to the results of Sec. 2.1, adding a free propagator which crosses from negative to positive light-cone time will however give only a zero contribution. Adding such a zero contribution it is then straight forward to Fourier transform our result back to momentum space. Therefore the complete amplitude can be calculated from the six diagrams of Fig. 4 with a vertex, Eqs. (15) and (16) at each cut, minus the diagram with the background field A^+ set to zero; if the initial particle is not colored (as in our case) the total number of diagrams reduces finally to four.

2.3 The minimal set of amplitudes

The final set of diagrams which we need to evaluate for the process described by Eq. (1) is depicted in Fig. 7. The four matrix elements corresponding to Fig. 7 read

$$\begin{aligned}
i\mathcal{A}_1 &= (ie)(ig) \int \frac{d^4k_1}{(2\pi)^4} \bar{u}(p) \gamma^\mu t^a \bar{S}_F(p+k, k_1) \gamma^\nu \bar{S}_F(k_1-l, -q) \\
& \quad \cdot [S_F^{(0)}(-q)]^{-1} v(q) \epsilon_\nu(l) \epsilon_\mu^*(k), \\
i\mathcal{A}_2 &= (ie)(ig) \int \frac{d^4k_1}{(2\pi)^4} \bar{u}(p) [S_F^{(0)}(p)]^{-1} \bar{S}_F(p, k_1) \gamma^\nu \bar{S}_F(k_1-l, -q-k) \\
& \quad \cdot \gamma^\mu t^a v(q), \epsilon_\nu(l) \epsilon_\mu^*(k), \\
i\mathcal{A}_3 &= (ie)(ig) \int \frac{d^4k_1}{(2\pi)^4} \int \frac{d^4k_2}{(2\pi)^4} \bar{u}(p) [S_F^{(0)}(p)]^{-1} \bar{S}_F(p, k_1-k_2) \gamma^\lambda t^c S_F^{(0)}(k_1) \gamma^\nu \\
& \quad \bar{S}_F(k_1-l, -q) [S_F^{(0)}(-q)]^{-1} v(q) [\bar{G}_\lambda^\delta]^{ca}(k_2, k) [G_\delta^{(0),\mu}(k)]^{-1} \epsilon_\nu(l) \epsilon_\mu^*(k), \\
i\mathcal{A}_4 &= (ie)(ig) \int \frac{d^4k_1}{(2\pi)^4} \int \frac{d^4k_2}{(2\pi)^4} \bar{u}(p) [S_F^{(0)}(p)]^{-1} \bar{S}_F(p, l-k_1) \gamma^\nu S_F^{(0)}(-k_1) \gamma^\lambda t^c \\
& \quad \bar{S}_F(k_2-k_1, -q) [S_F^{(0)}(-q)]^{-1} [\bar{G}_\lambda^\delta]^{ca}(k_2, k) [G_\delta^{(0),\mu}(k)]^{-1} \epsilon_\nu(l) \epsilon_\mu^*(k), \quad (17)
\end{aligned}$$

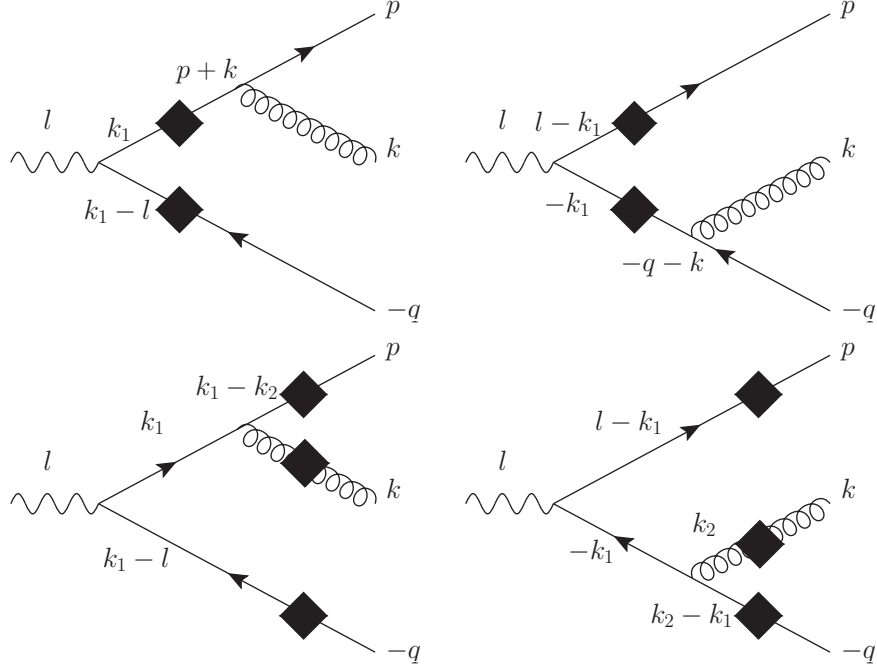


Figure 7: 3-parton production diagrams. The arrows indicate the direction of fermion charge flow. The photon momentum is incoming whereas all the final state momenta are outgoing.

where $\epsilon_\nu(l)$, $\epsilon_\mu^*(k)$ denote polarization vectors of the incoming virtual photon and the outgoing gluon respectively and

$$\begin{aligned}\bar{S}_{F,il}(p, q) &\equiv S_{F,ij}^{(0)}(p) \cdot \bar{\tau}_{F,jk}(p, q) \cdot S_{kl}^{(0)}(q), \\ \bar{G}_{\mu\nu}^{ad}(p, q) &\equiv G_{\mu\lambda}^{(0),ab}(p) \cdot \bar{\tau}_G^{bc}(p, q) \cdot G_\nu^{(0),cd,\lambda}(q)\end{aligned}\quad (18)$$

With flux factor $\mathcal{F} = 2l^+$, photon momentum fractions $\{z_1, z_2, z_3\} = \{p^+/l^+, q^+/l^+, k^+/l^+\}$, and the three-particle phase space,

$$\begin{aligned}d\Phi^{(3)} &= \frac{1}{(2\pi)^8} d^4p d^4q d^4k \delta(p^2) \delta(q^2) \delta(k^2) \delta(l^+ - p^+ - k^+ - q^+) \\ &= 2l^+ \frac{d^2\mathbf{p} d^2\mathbf{q} d^2\mathbf{k}}{(64\pi^4 l^+)^2} \frac{dz_1 dz_2 dz_3}{z_1 z_2 z_3} \delta(1 - \sum_{i=1}^3 z_i),\end{aligned}\quad (19)$$

the differential 3-parton production cross-section reads

$$d\sigma = \frac{1}{\mathcal{F}} \left\langle \left| \sum_{i=1}^4 \mathcal{M}_i(A^+) - \mathcal{M}_i(0) \right|^2 \right\rangle_{A^+} d\Phi^{(3)}, \quad (20)$$

where $\langle \dots \rangle_{A^+}$ denotes the average over background field configurations, $\mathcal{F} = 2l^+$ and

$$\mathcal{A}_i = 2\pi \delta(l^+ - p^+ - k^+ - q^+) \mathcal{M}_i \quad i = 1, \dots, 4. \quad (21)$$

3 Spinor helicity methods

While spinor helicity methods are well established for calculations within conventional perturbative QCD calculations, its application to calculations in the QCD high energy/Regge limit are rather limited, see [25] for some examples. We therefore start this section by recalling basic definitions which will further serve to fix our notation.

3.1 Basic definitions

The presentation in this paragraph follows closely those of the reviews [17]. For massless fermions, helicity is a good, *i.e.* conserved, quantum number. One defines (on-shell) helicity eigenstates (spinors) as

$$\begin{aligned} u_{\pm}(k) &= \frac{1 \pm \gamma_5}{2} u(p) & v_{\mp}(k) &= \frac{1 \pm \gamma_5}{2} v(p) \\ \bar{u}_{\pm}(k) &= \bar{u}(k) \frac{1 \mp \gamma_5}{2} & \bar{v}_{\pm}(k) &= \bar{v}(k) \frac{1 \pm \gamma_5}{2}. \end{aligned} \quad (22)$$

It is further convenient to introduce the following short-hands

$$|i^{\pm}\rangle \equiv |k_i^{\pm}\rangle \equiv u_{\pm}(k_i) = v_{\mp}(k_i) \quad \langle i^{\pm}| \equiv \langle k_i^{\pm}| \equiv \bar{u}_{\pm}(k_i) = \bar{v}_{\mp}(k_i) \quad (23)$$

Which allows to define the basic spinor products by

$$\langle k_i k_j \rangle \equiv \langle k_i^- | k_j^+ \rangle = \bar{u}_-(k_i) u_+(k_j), \quad [k_i k_j] \equiv \langle k_i^+ | k_j^- \rangle = \bar{u}_+(k_i) u_-(k_j). \quad (24)$$

Further note that

$$\langle k_i^{\pm} | k_j^{\pm} \rangle = 0 \quad \langle k_i^{\mp} | k_i^{\pm} \rangle = 0. \quad (25)$$

To evaluate such spinor products it is necessary to pick a certain representation of the Dirac γ matrices. In the Dirac representation

$$\gamma^0 = \begin{pmatrix} \mathbf{1} & \mathbf{0} \\ \mathbf{0} & -\mathbf{1} \end{pmatrix}, \quad \gamma^i = \begin{pmatrix} \mathbf{0} & \sigma^i \\ -\sigma^i & \mathbf{0} \end{pmatrix}, \quad \gamma^5 = \begin{pmatrix} \mathbf{0} & \mathbf{1} \\ \mathbf{1} & \mathbf{0} \end{pmatrix}. \quad (26)$$

with σ^i , $i = 1, \dots, 3$ the Pauli-matrices. Using the convention of Eq. (2) to define light-cone momenta, the massless spinors can be written as follows,

$$u_+(k) = v_-(k) = \frac{1}{2^{1/4}} \begin{pmatrix} \sqrt{k^+} \\ \sqrt{k^-} e^{i\phi_k} \\ \sqrt{k^+} \\ \sqrt{k^-} e^{i\phi_k} \end{pmatrix} \quad u_-(k) = v_+(k) = \frac{1}{2^{1/4}} \begin{pmatrix} \sqrt{k^-} e^{-i\phi_k} \\ -\sqrt{k^+} \\ -\sqrt{k^-} e^{-i\phi_k} \\ \sqrt{k^+} \end{pmatrix} \quad (27)$$

with

$$e^{i\phi_k} \equiv \frac{k^1 + ik^2}{\sqrt{k^2}} = \sqrt{2} \frac{\mathbf{k} \cdot \boldsymbol{\epsilon}}{\sqrt{k^2}}, \quad e^{-i\phi_k} = \sqrt{2} \frac{\mathbf{k} \cdot \boldsymbol{\epsilon}^*}{\sqrt{k^2}}, \quad \boldsymbol{\epsilon} = \frac{1}{\sqrt{2}}(1, i) \quad (28)$$

Using these expressions it is possible to obtain explicit formulae for the spinor brackets

$$\begin{aligned}
\langle k_i k_j \rangle &= \sqrt{2k_i^- k_j^+} e^{i\phi_{k_i}} - \sqrt{2k_j^- k_i^+} e^{i\phi_{k_j}} = \sqrt{2k_i^+ k_j^+} \left(\frac{\mathbf{k}_i \cdot \boldsymbol{\epsilon}}{k_i^+} - \frac{\mathbf{k}_j \cdot \boldsymbol{\epsilon}}{k_j^+} \right) \\
&= (k_i^+ k_j^+)^{-\frac{1}{2}} \left(k_j^+ |\mathbf{k}_i| e^{i\phi_{k_i}} - k_i^+ |\mathbf{k}_j| e^{i\phi_{k_j}} \right) \\
[k_i k_j] &= -\sqrt{2k_i^- k_j^+} e^{-i\phi_{k_i}} + \sqrt{2k_j^- k_i^+} e^{-i\phi_{k_j}} \\
&= -\sqrt{2k_i^+ k_j^+} \left(\frac{\mathbf{k}_i \cdot \boldsymbol{\epsilon}^*}{k_i^+} - \frac{\mathbf{k}_j \cdot \boldsymbol{\epsilon}^*}{k_j^+} \right) = -(k_i^+ k_j^+)^{-\frac{1}{2}} \left(k_j^+ |\mathbf{k}_i| e^{-i\phi_{k_i}} - k_i^+ |\mathbf{k}_j| e^{-i\phi_{k_j}} \right) \quad (29)
\end{aligned}$$

All of the above versions are equivalent to each other, but prove useful in specific circumstances. We further note that

$$2p \cdot k = \langle pk \rangle [kp], \quad [k_i k_i] = 0 = \langle k_i k_i \rangle, \quad \langle k_i k_j \rangle^* = -[k_i k_j], \quad (30)$$

where the last relation is particularly useful to invert helicities in an amplitude. While the above relations are valid in general, they are particularly useful for the description of high energy factorized amplitudes where light-cone momenta k_i^+ are conserved. In particular this enables us to deal with explicit expressions of brackets in the evaluation and leads to a further simplification of diagrams. For instance, for brackets involving light-cone vectors n, \bar{n} the following relations hold

$$\begin{aligned}
\langle n \bar{n} \rangle &= \sqrt{2}, & \langle np \rangle &= \sqrt{2p^+}, \\
[n \bar{n}] &= -\sqrt{2}, & [np] &= -\sqrt{2p^+}, \\
\langle \bar{n} p \rangle &= -\sqrt{2} \frac{\mathbf{p} \cdot \boldsymbol{\epsilon}}{\sqrt{p^+}}, & [\bar{n} p] &= \sqrt{2} \frac{\mathbf{p} \cdot \boldsymbol{\epsilon}^*}{\sqrt{p^+}}. \quad (31)
\end{aligned}$$

Since the (physical) Hilbert space of a massless vector is isomorphic to the Hilbert space of a massless spinor, it is further possible to express gluon and photon polarization vectors in terms of the above spinors. One has

$$\begin{aligned}
\epsilon_\mu^{(\lambda=+)}(k, n) &\equiv + \frac{\langle k^+ | \gamma_\mu | n^+ \rangle}{\sqrt{2} \langle n^- | k^+ \rangle} = \left(\epsilon_\mu^{(\lambda=-)}(k, n) \right)^*, \\
\epsilon_\mu^{(\lambda=-)}(k, n) &\equiv - \frac{\langle k^- | \gamma_\mu | n^- \rangle}{\sqrt{2} \langle n^+ | k^- \rangle} = \left(\epsilon_\mu^{(\lambda=+)}(k, n) \right)^*, \quad (32)
\end{aligned}$$

where k denotes the on-shell four-momentum of the boson and n the gauge vector. Obviously one has $\epsilon \cdot k = 0 = \epsilon \cdot n$. These polarization vectors obey the following polarization sum

$$\sum_{\lambda=\pm} \epsilon_\mu^{(\lambda)}(k, n) \left(\epsilon_\mu^{(\lambda)}(k, n) \right)^* = -g_{\mu\nu} + \frac{k_\mu n_\nu + n_\mu k_\nu}{k \cdot n}. \quad (33)$$

Using the Fierz identity,

$$\langle i^\pm | \gamma^\mu | j^\pm \rangle \langle k^\pm | \gamma_\mu | l^\pm \rangle = 2 \langle i^\pm | k^\mp \rangle \langle l^\mp | j^\pm \rangle, \quad (34)$$

polarization vectors contracted with Dirac matrices can be written as

$$\epsilon^\pm(k, n) = \frac{\pm\sqrt{2}}{\langle n^\mp | k^\pm \rangle} (|k^\mp\rangle\langle n^\mp| + |n^\pm\rangle\langle k^\pm|). \quad (35)$$

While the treatment of the real gluon is straight-forward within this formalism, the case of the virtual gluon is at first special. Since $l^2 = -Q^2 \neq 0$ in general, the photon has two transverse polarizations which are both annihilated by the light-cone vectors n, \bar{n} , *i.e.* one has $\epsilon_{\lambda=T}^\mu \cdot n = 0 = \epsilon_{\lambda=T}^\mu \cdot \bar{n}$. It is therefore straight forward to define transverse polarization vectors within the spinor helicity as

$$\epsilon_\mu^{(\lambda=\pm)}(l) \equiv \pm \frac{\langle \bar{n}^\pm | \gamma^\mu | n^\pm \rangle}{\sqrt{2} \langle n^\mp | \bar{n}^\pm \rangle}, \quad \text{with} \quad \sum_{\lambda=\pm} \epsilon_\mu^{(\lambda)}(l) \left(\epsilon_\nu^{(\lambda)}(l) \right)^* = -g_{\mu\nu}^t, \quad (36)$$

where $g_{\mu\nu}^t$ has only transverse components. The longitudinal polarization vector is given by

$$\epsilon_\mu^{(\lambda=L)}(l) \equiv \frac{1}{Q} \left[l^+ \bar{n}^\mu + \frac{Q^2}{2l^+} n^\mu \right]. \quad (37)$$

In the actual calculation we will make use of QED gauge invariance of the scattering amplitude and define

$$\bar{\epsilon}_\mu^{(\lambda=L)}(l) = \epsilon_\mu^{(\lambda=L)}(l) - \frac{1}{Q} l_\mu = \frac{Q}{l^+} n_\mu. \quad (38)$$

While adding a term proportional to l_μ will give a zero contribution upon contraction with the amplitude, the above form will facilitate actual calculations.

3.2 Calculation of amplitudes

To evaluate the set of amplitudes Eq. (17) we first note that due to the usual spin sums of spinors we have for any on-shell momentum $p^2 = 0$

$$\not{p} = |p^+\rangle\langle p^+| + |p^-\rangle\langle p^-|, \quad (39)$$

which allows us to expand contractions of gamma matrices with momenta p, q, k of the final state particles as well as with the light-cone vectors n, \bar{n} in terms of spinors. For the momentum of the initial state off-shell photon we use the representation in Eq. (3) and apply Eq. (39) to each of the light-cone vectors. For the internal momentum $k_{1,2}$, which are integrated over and which are therefore intrinsically off-shell, we use the following decomposition

$$k_{1,2}^\mu = \bar{k}_{1,2}^\mu + \frac{k_{1,2}^2}{2k_{1,2}^+} n^\mu \quad \text{with} \quad \bar{k}_{1,2}^\mu = k_{1,2}^+ \bar{n}^\mu + \frac{\mathbf{k}_{1,2}^2}{2k_{1,2}^+} n^\mu + k_{1,2;t}^\mu; \quad (40)$$

since $\bar{k}_{1,2}^2 = 0$, both vectors used to represent $k_{1,2}$ have a spinor representation. While there are many possibilities to present a massive four vector in terms of two mass-less four-vectors, the above presentation has two advantages that make it special: a) since plus-momenta are conserved during interaction with the background field, the denominators introduced in Eq. (40) can be directly expressed in terms of plus momenta of external particles b) making

use of Eq. (25) and the fact that Eq. (15) is directly proportional to \not{n} , terms proportional to n^μ will be set to zero in most cases. To keep our notation more compact, we further use

$$l^\mu = \bar{l}^\mu - \frac{Q^2}{2l^+} n^\mu \quad \text{with} \quad \bar{l}^\mu = l^+ \bar{n}^\mu \quad (41)$$

In the case of gluons a similar simplifications can be achieved using the decomposition of Eq. (40), since

$$d^{\mu\nu}(k_2) = -g^{\mu\nu} + \frac{\bar{k}_2^\mu n^\nu + \bar{k}_2^\nu n^\mu}{\bar{k}_2 \cdot n} + \frac{n^\mu n^\nu k_2^2}{2(n \cdot k_2)^2}. \quad (42)$$

For the current calculation the gluon polarization tensor will be always contracted with an external polarization vector. In this case one finds

$$d^{\mu\nu}(k_2) \cdot \epsilon_\nu^{\lambda,*}(k) = -\epsilon_\mu^{\lambda,*}(\bar{k}_2) \quad (43)$$

where we made use of the polarization sum, Eq. (33), and

$$\epsilon_\nu^\pm(\bar{k}_2) \cdot \epsilon_\nu^{\pm,*}(k) = -\frac{\langle \bar{k}_2^\pm | n^\mp \rangle \langle k^\mp | n^\pm \rangle}{\langle n^\pm | k^\mp \rangle \langle n^\mp | \bar{k}_2^\pm \rangle} = -1 \quad \epsilon_\nu^\pm(\bar{k}_2) \cdot \epsilon_\nu^{\mp,*}(k) = 0. \quad (44)$$

Equipped with this information, evaluation of the numerators of the diagrams Eq. (17) is straight forward. While a direct evaluation is possible – most efficiently done using Computer algebra systems – the spinor helicity formalism allows to break down the calculation into independent sub-amplitudes, which allows for a very economic evaluation. In the following we explain this in full detail using diagram 1 and 3 as examples; the case of diagram 2 and 4 follows then directly.

3.3 Evaluation of diagrams 1 and 3

To put all the relations above to work and get some practice with the spinor helicity methods, we consider at first the first and third diagrams given by $i\mathcal{A}_1$ and $i\mathcal{A}_3$. We have

$$i\mathcal{A}_1^a = eg \int d^2\mathbf{x}_1 d^2\mathbf{x}_2 \int \frac{d^4 k_1}{(2\pi)^2} e^{i(\mathbf{k}_1 - \mathbf{p} - \mathbf{k}) \cdot \mathbf{x}_1} e^{-i(\mathbf{k}_1 + \mathbf{q}) \cdot \mathbf{x}_2} \delta(p^+ + k^+ - k_1^+) \delta(k_1^+ - l^+ + q^+) \cdot t^a V(x_{1,t}) V^\dagger(x_{2,t}) \cdot \frac{-i \cdot N_1}{k_1^2 (k_1 - l)^2}, \quad (45)$$

where N_1 is the numerator which further includes the denominator of the external quark line

$$N_1^{\lambda_\gamma; \lambda_q \lambda_{\bar{q}} \lambda_g} = \frac{1}{(p+k)^2} \cdot \bar{u}_{\lambda_q}(p) \left(\not{\epsilon}^{(\lambda_g)} \right)^* (k) (\not{p} + \not{k}) \not{k}_1 \not{\epsilon}^{(\lambda_\gamma)}(l) (\not{k}_1 - \not{l}) \not{l} v_{\lambda_{\bar{q}}}(q). \quad (46)$$

Here $\lambda_\gamma = (L, T = \pm)$, $\lambda_q = (\pm)$, $\lambda_{\bar{q}} = (\pm)$, $\lambda_g = (\pm)$ encode the possible helicity states of initial and final state particles. In the case of amplitude 3 we find

$$i\mathcal{A}_3^a = eg \prod_{j=1}^3 \int d^2\mathbf{x}_j \int \frac{d^4 k_1 d^4 k_2}{(2\pi)^5} e^{i(\mathbf{k}_1 - \mathbf{k}_2 - \mathbf{p}) \cdot \mathbf{x}_1} e^{-i(\mathbf{k}_1 + \mathbf{q}) \cdot \mathbf{x}_2} e^{i(\mathbf{k}_2 - \mathbf{k}) \cdot \mathbf{x}_3} \delta(p^+ - k_1^+ + k_2^+) \delta(k_1^+ - l^+ + q^+) \delta(k_2^+ - k^+) \cdot V(x_t) t^b V^\dagger(y_t) U(z_t)^{ba} \frac{(-2k^+) N_3}{[(k_1 - k_2)^2 + i\epsilon][k_1^2 + i\epsilon][k_2^2 + i\epsilon][(k - l)^2 + i\epsilon]}, \quad (47)$$

with N_3 defined as

$$N_3^{\lambda_\gamma; \lambda_q \lambda_{\bar{q}} \lambda_g} = \bar{u}_{\lambda_q} \not{k}_1 (\not{k}_1 - \not{k}_2) \left(\not{\epsilon}^{(\lambda_g)} \right)^* (k_2) \not{k}_1 \not{\epsilon}^{(\lambda_\gamma)} (l) (\not{k}_1 - \not{l}) \not{v}_{\lambda_{\bar{q}}} (q). \quad (48)$$

It is now possible to factorize both N_1 and N_3 which in turn will allow for their efficient evaluation. To this end we split $N_{1,3}$ into two, using the spinor representation of \not{k}_1 , which itself relies on the decomposition in Eq. (40). Note that in this decomposition the term proportional to \not{l} gives a zero result for N_1 . We therefore have²

$$\begin{aligned} N_1^{\lambda_\gamma; \lambda_q \lambda_{\bar{q}} \lambda_g} &= Q_{\gamma^* \rightarrow q \bar{q}}^{\lambda_\gamma \lambda_q}(\bar{k}_1) \cdot Q_{q \rightarrow qg}^{\lambda_q \lambda_g; 1}(\bar{k}_1), \\ N_3^{\lambda_\gamma; \lambda_q \lambda_{\bar{q}} \lambda_g} &= Q_{\gamma^* \rightarrow q \bar{q}}^{\lambda_\gamma \lambda_q}(\bar{k}_1) \cdot Q_{q \rightarrow qg}^{\lambda_q \lambda_g; 3}(\bar{k}_1) + \frac{k_1^2}{2k_1^+} \cdot Q_{\gamma^* \rightarrow q \bar{q}}^{\lambda_\gamma \lambda_q}(n) \cdot Q_{q \rightarrow qg}^{\lambda_q \lambda_g; 3}(n), \end{aligned} \quad (49)$$

where

$$\begin{aligned} Q_{\gamma^* \rightarrow q \bar{q}}^{\lambda_\gamma \lambda_q}(\bar{k}_1) &= \bar{u}_{\lambda_q}(\bar{k}_1) \not{\epsilon}^{(\lambda_\gamma)}(l) (\not{k}_1 - \not{l}) \not{v}_{\lambda_{\bar{q}}}(q), \\ Q_{q \rightarrow qg}^{\lambda_q \lambda_g; 1}(\bar{k}_1) &= \frac{1}{(p+k)^2} \cdot \bar{u}_{\lambda_q}(p) \left(\not{\epsilon}^{(\lambda_g)} \right)^* (k) (\not{p} + \not{k}) \not{u}_{\lambda_q}(\bar{k}_1), \\ Q_{q \rightarrow qg}^{\lambda_q \lambda_g; 3}(\bar{k}_1) &= \bar{u}_{\lambda_q} \not{k}_1 (\not{k}_1 - \not{k}_2) \left(\not{\epsilon}^{(\lambda_g)} \right)^* (k_2) u_{\lambda_q}(\bar{k}_1). \end{aligned} \quad (50)$$

We start with the splitting $\gamma^* \rightarrow q \bar{q}$, with configuration where the incoming photon has longitudinal polarization ($\lambda = L$). We find

$$\begin{aligned} Q_{\gamma^* \rightarrow q \bar{q}}^{L+}(\bar{k}_1) &= \frac{Q}{l^+} [\bar{k}_1 n] (\langle n \bar{k}_1 \rangle [\bar{k}_1 n] - \langle n \bar{l} \rangle [\bar{l} n]) \langle n q \rangle, \\ &= -4 \frac{Q}{l^+} (p^+ + k^+)^{\frac{1}{2}} (q^+)^{\frac{3}{2}}, \\ Q_{\gamma^* \rightarrow q \bar{q}}^{L+}(n) &= 0, \\ Q_{\gamma^* \rightarrow q \bar{q}}^{L-}(\bar{k}_1) &= \left(Q_{\gamma^* \rightarrow q \bar{q}}^{L+}(\bar{k}_1) \right)^* = Q_{\gamma^* \rightarrow q \bar{q}}^{L+}(\bar{k}_1), \end{aligned} \quad (51)$$

where we made use of Eq. (30) to invert the helicities in the last expression. For transverse photon polarizations $T = \pm$ we find

$$\begin{aligned} Q_{\gamma^* \rightarrow q \bar{q}}^{++}(\bar{k}_1) &= \frac{\sqrt{2}}{\langle n \bar{n} \rangle} [\bar{k}_1 \bar{n}] (\langle n \bar{k}_1 \rangle [\bar{k}_1 n] - \langle n \bar{l} \rangle [\bar{l} n]) \langle n q \rangle = 4 \mathbf{k}_1 \cdot \boldsymbol{\epsilon}^* \frac{(q^+)^{\frac{3}{2}}}{(p^+ + k^+)^{\frac{1}{2}}}, \\ Q_{\gamma^* \rightarrow q \bar{q}}^{+-}(\bar{k}_1) &= \frac{\sqrt{2}}{\langle n \bar{n} \rangle} \langle \bar{k}_1 n \rangle [\bar{n} \bar{k}_1] \langle \bar{k}_1 n \rangle [n q] = -4 \mathbf{k}_1 \cdot \boldsymbol{\epsilon}^* (p^+ + k^+)^{\frac{1}{2}} (q^+)^{\frac{1}{2}}, \\ Q_{\gamma^* \rightarrow q \bar{q}}^{++}(n) &= 4 (q^+)^{\frac{3}{2}}, & Q_{\gamma^* \rightarrow q \bar{q}}^{+-}(n) &= 0, \\ Q_{\gamma^* \rightarrow q \bar{q}}^{+-}(\bar{k}_1) &= \left(Q_{\gamma^* \rightarrow q \bar{q}}^{+-}(\bar{k}_1) \right)^*, & Q_{\gamma^* \rightarrow q \bar{q}}^{--}(\bar{k}_1) &= \left(Q_{\gamma^* \rightarrow q \bar{q}}^{++}(\bar{k}_1) \right)^*. \end{aligned} \quad (52)$$

For the splitting $q \rightarrow qg$ it is obviously necessary to distinguish between amplitude one (interaction before the splitting) and three (interaction after the splitting). For the first case

²Recall that the helicity of the anti-quark is due to helicity conservation in massless QCD always opposite to the quark helicity $\lambda_{\bar{q}} = -\lambda_q$

we obtain

$$\begin{aligned}
Q_{q \rightarrow qg}^{++;1} &= -\frac{\sqrt{2}[pn][pn]\langle n\bar{k}_1 \rangle}{[nk][pk]} = \frac{2^{\frac{3}{2}} \cdot (p^+)^{\frac{3}{2}}(p^+ + k^+)^{\frac{1}{2}}}{p^+|\mathbf{k}|e^{-i\phi_k} - k^+|\mathbf{p}|e^{-i\phi_p}}, \\
Q_{q \rightarrow qg}^{+-;1} &= \frac{\sqrt{2}(\langle np \rangle[pn] + \langle nk \rangle[kn])\langle n\bar{k}_1 \rangle}{\langle nk \rangle \langle kp \rangle} = \frac{2^{\frac{3}{2}} \cdot (p^+)^{\frac{1}{2}}(p^+ + k^+)^{\frac{3}{2}}}{p^+|\mathbf{k}|e^{i\phi_k} - k^+|\mathbf{p}|e^{i\phi_p}}, \\
Q_{q \rightarrow qg}^{--;1} &= (Q_{q \rightarrow qg}^{++;1})^*, \quad Q_{q \rightarrow qg}^{-+;1} = (Q_{q \rightarrow qg}^{+-;1})^*,
\end{aligned} \tag{53}$$

where we used $(p+k)^2 = [pk]\langle kp \rangle$. Note that these splittings allow for a straight forward identification (and if needed isolation) of collinear and soft singularities. Indeed, these splittings encode (together with the corresponding $\bar{q} \rightarrow \bar{q}g$ splittings in amplitude 2) the complete soft ($k \rightarrow 0$) and collinear ($k \propto p$) singularities of the process, corresponding to the vanishing of the brackets $\langle p^\pm | k^\mp \rangle$. The corresponding splitting which occurs in the third amplitude is on the other hand free of such potentially singular configurations. One finds³

$$\begin{aligned}
Q_{q \rightarrow qg}^{(++)3}(\bar{k}_1) &= \frac{\sqrt{2} \cdot [pn](\langle n\bar{k}_1 \rangle[\bar{k}_1 n] - \langle n\bar{k}_2 \rangle[\bar{k}_2 n])\langle \bar{k}_2 \bar{k}_1 \rangle}{[n\bar{k}_2]} \\
&= 4(p^+)^{\frac{3}{2}}(p^+ + k^+)^{\frac{1}{2}} \left(\frac{\mathbf{k}_1 \cdot \boldsymbol{\epsilon}}{p^+ + k^+} - \frac{\mathbf{k}_2 \cdot \boldsymbol{\epsilon}}{k^+} \right), \\
Q_{q \rightarrow qg}^{(+-)3}(\bar{k}_1) &= -\frac{\sqrt{2}}{\langle n\bar{k}_2 \rangle} [pn] \langle n\bar{k}_1 \rangle [\bar{k}_1 \bar{k}_2] \langle n\bar{k}_1 \rangle \\
&= 4(p^+)^{\frac{1}{2}}(p^+ + k^+)^{\frac{3}{2}} \left(\frac{\mathbf{k}_1 \cdot \boldsymbol{\epsilon}^*}{p^+ + k^+} - \frac{\mathbf{k}_2 \cdot \boldsymbol{\epsilon}^*}{k^+} \right) \\
Q_{q \rightarrow qg}^{(++)3}(n) &= \frac{\sqrt{2} \cdot [pn](\langle n\bar{k}_1 \rangle[\bar{k}_1 n] - \langle n\bar{k}_2 \rangle[\bar{k}_2 n])\langle \bar{k}_2 n \rangle}{[n\bar{k}_2]} = 4(p^+)^{\frac{3}{2}}, \\
Q_{q \rightarrow qg}^{(+-)3}(n) &= 0, \quad Q_{q \rightarrow qg}^{--;3} = (Q_{q \rightarrow qg}^{++;3})^*, \quad Q_{q \rightarrow qg}^{-+;3} = (Q_{q \rightarrow qg}^{+-;3})^*.
\end{aligned} \tag{54}$$

3.4 Diagrams 2 and 4 from symmetry

The corresponding expressions for diagrams 2 and 4 read:

$$\begin{aligned}
i\mathcal{A}_2^a &= eg \int d^2\mathbf{x}_1 d^2\mathbf{x}_2 \int \frac{d^4k_1}{(2\pi)^2} e^{-i(\mathbf{q}+\mathbf{k}-\mathbf{k}_1)\cdot\mathbf{x}_2} e^{-i(\mathbf{k}_1+\mathbf{p})\cdot\mathbf{x}_1} \\
&\delta(q^+ + k^+ - k_1^+) \delta(k_1^+ - l^+ + p^+) \cdot V(x_{1,t}) V^\dagger(x_{2,t}) t^a \cdot \frac{-i \cdot N_2}{k_1^2 (k_1 - l)^2},
\end{aligned} \tag{55}$$

where N_2 is the numerator which further includes the denominator of the external anti-quark line

$$N_2^{\lambda_\gamma; \lambda_q \lambda_{\bar{q}} \lambda_g} = \frac{1}{(q+k)^2} \cdot \bar{u}_{\lambda_q}(p) \not{\ell} (\not{l} - \not{k}_1) \not{\epsilon}^{(\lambda_\gamma)}(l) (-\not{k}_1) \not{\ell} (-\not{q} - \not{k}) \left(\not{\epsilon}^{(\lambda_g)} \right)^* (k) v_{\lambda_{\bar{q}}}(q), \tag{56}$$

³Note that in slight abuse of notation, the argument \bar{k}_1 is meant to apply only to the very last spinor in the chain

and

$$i\mathcal{A}_4^a = eg \prod_{j=1}^3 \int d^2 x_j \int \frac{d^4 k_1 d^4 k_2}{(2\pi)^5} e^{-i(\mathbf{q}-\mathbf{k}_1+\mathbf{k}_2)\cdot\mathbf{x}_2} e^{-i(\mathbf{k}_1+\mathbf{p})\cdot\mathbf{x}_1} e^{+i(\mathbf{k}_2-\mathbf{k})\cdot\mathbf{x}_3} \\ \delta(q^+ - k_1^+ + k_2^+) \delta(k_1^+ - l^+ + p^+) \delta(k_2^+ - k^+) \cdot V(x_{1,t}) t^b V^\dagger(x_{2,t}) U(x_{3,t})^{ba} \\ \frac{(-2k^+) N_4}{[(k_1 - k_2)^2 + i\epsilon][k_1^2 + i\epsilon][k_2^2 + i\epsilon][(k_1 - l)^2 + i\epsilon]}, \quad (57)$$

with N_4 defined as

$$N_4^{\lambda_\gamma; \lambda_q \lambda_{\bar{q}} \lambda_g} = \bar{u}_{\lambda_q}(p) \not{\epsilon}(\not{l} - \not{k}_1) \not{\epsilon}^{(\lambda_\gamma)}(l) \not{k}_1 \left(\not{\epsilon}^{(\lambda_g)} \right)^* (k_2) (\not{k}_2 - \not{k}_1) \not{\epsilon} v_{\lambda_{\bar{q}}}(q). \quad (58)$$

Expanding $N_{2,4}$ in terms of spinors one realizes immediately that the resulting expression is identical to $N_{1,3}$ up to a) interchange of momenta $p \leftrightarrow q$ b) the order in which spinors are written and c) a minus sign for each propagator numerator. In particular one finds the following factorization of N_2 and N_4 :

$$N_2^{\lambda_\gamma; \lambda_q \lambda_{\bar{q}} \lambda_g} = -\bar{Q}_{\gamma^* \rightarrow q\bar{q}}^{\lambda_\gamma \lambda_q}(\bar{k}_1) \cdot Q_{\bar{q} \rightarrow \bar{q}g}^{\lambda_q \lambda_g; 2}(\bar{k}_1), \\ N_4^{\lambda_\gamma; \lambda_q \lambda_{\bar{q}} \lambda_g} = -\bar{Q}_{\gamma^* \rightarrow q\bar{q}}^{\lambda_\gamma \lambda_q}(\bar{k}_1) \cdot Q_{\bar{q} \rightarrow \bar{q}g}^{\lambda_q \lambda_g; 4}(\bar{k}_1) - \bar{Q}_{\gamma^* \rightarrow q\bar{q}}^{\lambda_\gamma \lambda_q}(n) \cdot Q_{\bar{q} \rightarrow \bar{q}g}^{\lambda_q \lambda_g; 4}(n), \quad (59)$$

where

$$\bar{Q}_{\gamma^* \rightarrow q\bar{q}}^{\lambda_\gamma \lambda_q}(\bar{k}_1) = \bar{u}_{\lambda_q}(p) \not{\epsilon}(\not{k}_1 - \not{l}) \not{\epsilon}^{(\lambda_\gamma)}(l) v_{\lambda_{\bar{q}}}(\bar{k}_1), \\ Q_{\bar{q} \rightarrow \bar{q}g}^{\lambda_q \lambda_g; 2}(\bar{k}_1) = \frac{1}{(q+k)^2} \cdot \bar{u}_{\lambda_q}(\bar{k}_1) \not{\epsilon} \left(\not{\epsilon}^{(\lambda_g)} \right)^* (k) (-\not{q} - \not{k}) v_{\lambda_{\bar{q}}}(q) \\ Q_{\bar{q} \rightarrow \bar{q}g}^{\lambda_q \lambda_g; 4}(\bar{k}_1) = \bar{u}_{\lambda_q}(\bar{k}_1) \left(\not{\epsilon}^{(\lambda_g)} \right)^* (k_2) \not{\epsilon}(\not{k}_2 - \not{k}_1) \not{\epsilon} v_{\lambda_{\bar{q}}}(q). \quad (60)$$

Evaluating these expressions one realizes, that they are identical to the corresponding expressions of diagrams 1 and 3, up to $q \leftrightarrow p$ and an overall minus sign (due to the different sign in the numerator of the internal propagators). In case of the $\bar{q} \rightarrow \bar{q}g$ splitting of diagram 2 we find for instance

$$Q_{\bar{q} \rightarrow \bar{q}g}^{-+; 2}(\bar{k}_1) = \frac{\sqrt{2}}{[nk][kq]} \langle \bar{k}_1 n \rangle [nq][nq]. \quad (61)$$

Using now anti-symmetry of the brackets in the numerator as well as the bracket $[kq]$ in the denominator, this expression can be transformed into⁴

$$Q_{\bar{q} \rightarrow \bar{q}g}^{(-+; 2)}(\bar{k}_1) = \frac{\sqrt{2}[qn][qn]\langle nk_1 \rangle}{[nk][qk]} = -Q_{q \rightarrow qg}^{(++; 1)}(\bar{k}_1; q \leftrightarrow p). \quad (62)$$

We therefore find that the corresponding expressions of diagrams 2 and 4 can be obtained from the corresponding ones of diagram 1 and 3 through a) inverting the quark helicity b) interchanging momenta p and q and c) an overall minus sign. In detail we have

$$\bar{Q}_{\gamma^* \rightarrow q\bar{q}}^{(\lambda_\gamma \lambda_q)}(\bar{k}_1) = -Q_{\gamma^* \rightarrow q\bar{q}}^{(\lambda_\gamma (-\lambda_q))}(\bar{k}_1; p \leftrightarrow q), \\ Q_{\bar{q} \rightarrow \bar{q}g}^{(\lambda_q \lambda_g; 2)}(\bar{k}_1) = -Q_{q \rightarrow \bar{q}g}^{(-\lambda_q \lambda_g; 1)}(\bar{k}_1; p \leftrightarrow q), \\ Q_{\bar{q} \rightarrow \bar{q}g}^{(\lambda_q \lambda_g; 4)}(\bar{k}_1) = -Q_{q \rightarrow \bar{q}g}^{(-\lambda_q \lambda_g; 3)}(\bar{k}_1; p \leftrightarrow q). \quad (63)$$

⁴ recall that an anti-quark spinor with positive (negative) helicity is identical to a quark spinor with negative (positive) helicity

3.5 Wilson lines and color algebra

To this end we recall that the amplitudes in Eq. (17) carry both fundamental and adjoint color indices. Making color indices of the fundamental representation explicit, we have $\mathcal{A}_{\#,ij}^a$ where $\# = 1, \dots, 4$. To write down the differential cross-section we are in general dealing with expressions of the form

$$\mathcal{A}_{\#1,ij}^a \mathcal{A}_{\#2,ij}^{a,\dagger}, \quad \#_i = 1, \dots, 4 \quad (64)$$

with indices a, i, j summed over. It is now convenient to rewrite this as

$$\mathcal{A}_{\#1,ij}^a \mathcal{A}_{\#2,ij}^{a,\dagger} = 2\mathcal{A}_{\#1,ij}^a t_{kl}^a t_{lk}^b \mathcal{A}_{\#2,ij}^{b,\dagger}, \quad (65)$$

which allows us to define amplitudes with four fundamental color indices only. Extracting factors of Wilson lines and $SU(N_c)$ generators, we find in this way

$$\begin{aligned} \left[V^\dagger(\mathbf{x}_2) V(\mathbf{x}_1) t_{ij}^a \right] t_{kl}^a &= \frac{1}{2} \left[V^\dagger(\mathbf{x}_2) V(\mathbf{x}_1) \right]_{il} \delta_{jk} - \frac{1}{2N_c} \left[V^\dagger(\mathbf{x}_2) V(\mathbf{x}_1) \right]_{ij} \delta_{kl} \\ \left[t_{ij}^a V^\dagger(\mathbf{x}_2) V(\mathbf{x}_1) \right] t_{kl}^a &= \frac{1}{2} \delta_{il} \left[V^\dagger(\mathbf{x}_2) V(\mathbf{x}_1) \right]_{jk} - \frac{1}{2N_c} \left[V^\dagger(\mathbf{x}_2) V(\mathbf{x}_1) \right]_{ij} \delta_{kl} \\ \left[V^\dagger(\mathbf{x}_2) t_{ij}^b V(\mathbf{x}_1) \right] U^{ab}(\mathbf{x}_3) t_{kl}^a &= \left[V^\dagger(\mathbf{x}_2) V(\mathbf{x}_3) t_{ij}^a V^\dagger(\mathbf{x}_3) V(\mathbf{x}_1) \right]_{ij} t_{kl}^a \\ &= \frac{1}{2} \left[V^\dagger(\mathbf{x}_2) V(\mathbf{x}_3) \right]_{il} \left[V^\dagger(\mathbf{x}_3) V(\mathbf{x}_1) \right]_{kj} - \frac{1}{2N_c} \left[V^\dagger(\mathbf{x}_2) V(\mathbf{x}_1) \right]_{ij} \delta_{kl} \end{aligned} \quad (66)$$

where the first two lines corresponds to diagram one and two respectively while the last line gives the corresponding factor of diagrams three and four. To determine the operators of Wilson lines at cross-section level, we restrict at first to the leading N_c terms and subtract contributions without target interaction (as indicated in Eq. (20)). Extracting an overall factor $N_c^2/2$ and using the conventional definitions of dipole and quadrupole

$$S_{(\mathbf{x}_1 \mathbf{x}_2)}^{(2)} \equiv \frac{1}{N_c} \text{tr} \left[V(\mathbf{x}_1) V^\dagger(\mathbf{x}_2) \right], \quad S_{(\mathbf{x}_1 \mathbf{x}_2 \mathbf{x}_3 \mathbf{x}_4)}^{(4)} \equiv \frac{1}{N_c} \text{tr} \left[V(\mathbf{x}_1) V^\dagger(\mathbf{x}_2) V(\mathbf{x}_3) V^\dagger(\mathbf{x}_4) \right], \quad (67)$$

we obtain the following set of operators,

$$\begin{aligned} N^{(4)}(\mathbf{x}_1, \mathbf{x}_2, \mathbf{x}_3, \mathbf{x}_4) &\equiv 1 + S_{(\mathbf{x}_1 \mathbf{x}_2 \mathbf{x}_3 \mathbf{x}_4)}^{(4)} - S_{(\mathbf{x}_1 \mathbf{x}_2)}^{(2)} - S_{(\mathbf{x}_3 \mathbf{x}_4)}^{(2)}, \\ N^{(22)}(\mathbf{x}_1, \mathbf{x}_2 | \mathbf{x}_3, \mathbf{x}_4) &\equiv \left[S_{(\mathbf{x}_1 \mathbf{x}_2)}^{(2)} - 1 \right] \left[S_{(\mathbf{x}_3 \mathbf{x}_4)}^{(2)} - 1 \right] \\ N^{(24)}(\mathbf{x}_1, \mathbf{x}_2 | \mathbf{x}_3, \mathbf{x}_4, \mathbf{x}_5, \mathbf{x}_6) &\equiv 1 + S_{(\mathbf{x}_1 \mathbf{x}_2)}^{(2)} S_{(\mathbf{x}_3 \mathbf{x}_4 \mathbf{x}_5 \mathbf{x}_6)}^{(4)} - S_{(\mathbf{x}_1 \mathbf{x}_2)}^{(2)} S_{(\mathbf{x}_3 \mathbf{x}_6)}^{(2)} - S_{(\mathbf{x}_4 \mathbf{x}_5)}^{(2)}, \\ N^{(44)}(\mathbf{x}_1, \mathbf{x}_2, \mathbf{x}_3, \mathbf{x}_4 | \mathbf{x}_5, \mathbf{x}_6, \mathbf{x}_7, \mathbf{x}_8) &\equiv 1 + S_{(\mathbf{x}_1 \mathbf{x}_2 \mathbf{x}_3 \mathbf{x}_4)}^{(4)} S_{(\mathbf{x}_5 \mathbf{x}_6 \mathbf{x}_7 \mathbf{x}_8)}^{(4)} \\ &\quad - S_{(\mathbf{x}_1 \mathbf{x}_4)}^{(2)} S_{(\mathbf{x}_5 \mathbf{x}_8)}^{(2)} - S_{(\mathbf{x}_2 \mathbf{x}_3)}^{(2)} S_{(\mathbf{x}_6 \mathbf{x}_7)}^{(2)}, \end{aligned} \quad (68)$$

which are used to write down our final result for the differential cross-section Eq. (73). To obtain sub-leading terms in N_c , the operators $N^{(4)}, N^{(22)}, N^{(24)}, N^{(44)}$ need to be replaced by $1/N_c \cdot N^{(4)}(\mathbf{x}_1, \mathbf{x}_1', \mathbf{x}_2', \mathbf{x}_2)$.

Diffractive reactions (where the color exchange is at amplitude level restricted to the color singlet) require to project the $q\bar{q}g$ system onto an overall color-singlet. This leads to the following replacement of Eq. (64)

$$\mathcal{A}_{\#1,ij}^a P_{ji;i'j'}^{ab} \mathcal{A}_{\#2,i'j'}^{a,\dagger} = 2\mathcal{A}_{\#1,ij}^a t_{ji}^a t_{i'j'}^b \mathcal{A}_{\#2,i'j'}^{b,\dagger}. \quad (69)$$

At the level of Eq. (66) this corresponds to replacing t_{kl}^a by t_{ji}^a on the right-hand side which translates into contracting the left-hand side with $\delta_{jk}\delta_{li}$. As a results one finds that all quadrupole operators in Eq. (68) factorize into a product of dipole operators. One finds for the leading N_c terms:

$$\begin{aligned} N_{\text{diff}}^{(4)}(\mathbf{x}_1, \mathbf{x}_2, \mathbf{x}_3, \mathbf{x}_4) &\equiv \left[1 - S_{(\mathbf{x}_1\mathbf{x}_2)}^{(2)}\right] \left[1 - S_{(\mathbf{x}_3\mathbf{x}_4)}^{(2)}\right], \\ N_{\text{diff}}^{(22)}(\mathbf{x}_1, \mathbf{x}_2|\mathbf{x}_3, \mathbf{x}_4) &\equiv \left[S_{(\mathbf{x}_1\mathbf{x}_2)}^{(2)} - 1\right] \left[S_{(\mathbf{x}_3\mathbf{x}_4)}^{(2)} - 1\right], \\ N_{\text{diff}}^{(24)}(\mathbf{x}_1, \mathbf{x}_2|\mathbf{x}_3, \mathbf{x}_4, \mathbf{x}_5, \mathbf{x}_6) &\equiv \left[1 - S_{(\mathbf{x}_1\mathbf{x}_2)}^{(2)} S_{(\mathbf{x}_3\mathbf{x}_6)}^{(2)}\right] \left[1 - S_{(\mathbf{x}_4\mathbf{x}_5)}^{(2)}\right], \\ N_{\text{diff}}^{(44)}(\mathbf{x}_1, \mathbf{x}_2, \mathbf{x}_3, \mathbf{x}_4|\mathbf{x}_5, \mathbf{x}_6, \mathbf{x}_7, \mathbf{x}_8) &\equiv \left[1 - S_{(\mathbf{x}_1\mathbf{x}_4)}^{(2)} S_{(\mathbf{x}_5\mathbf{x}_8)}^{(2)}\right] \left[1 - S_{(\mathbf{x}_2\mathbf{x}_3)}^{(2)} S_{(\mathbf{x}_6\mathbf{x}_7)}^{(2)}\right]. \end{aligned} \quad (70)$$

To obtain sub-leading terms in N_c , it is again necessary to replace the operators $N_{\text{diff}}^{(4)}$, $N_{\text{diff}}^{(22)}$, $N_{\text{diff}}^{(24)}$, $N_{\text{diff}}^{(44)}$ by $1/N_c \cdot N_{\text{diff}}^{(4)}(\mathbf{x}_1, \mathbf{x}_{1'}, \mathbf{x}_{2'}, \mathbf{x}_2)$.

3.6 Integrals

Integrations over plus-momenta are carried out trivially using the delta-functions associated with the vertices Eqs. (15) and (16). Integrations over minus-momenta can be performed using contour integrations. In the case of diagram one and two one finds

$$\begin{aligned} I_1 &= -i \int \frac{dk_1^+}{2\pi} \int \frac{dk_1^-}{2\pi} \frac{(2\pi)^2 \delta(p^+ - k^+ - k_1^+) \delta(k_1^+ - l^+ - q^+)}{[k_1^2 + i\epsilon][(k_1 - l)^2 + i\epsilon]} \\ &= 2\pi \delta(l^+ - p^+ - k^+ - q^+) \frac{1}{2l^+} \frac{1}{[k_{1t}^2 + z_2(z_1 + z_3)Q^2]} \\ I_2 &= I_1 (\{p^+ \leftrightarrow q^+\}) \end{aligned} \quad (71)$$

with photon momentum fractions $z_1 = p^+/l^+$, $z_2 = q^+/l^+$ and $z_3 = k^+/l^+$. In the case of diagrams three and four two (closely related) integrals are needed for each diagram. One has

$$\begin{aligned}
I_{3,1} &= \int \frac{dk_1^+}{2\pi} \int \frac{dk_2^+}{2\pi} \int \frac{dk_1^-}{2\pi} \int \frac{dk_2^-}{2\pi} (2\pi)^3 \delta(p^+ - k_1^+ + k_2^+) \delta(k_1^+ - l^+ + q^+) \delta(k_2^+ - k^+) \\
&\quad \cdot \frac{(-2k^+)}{[(k_1 - k_2)^2 + i\epsilon][k_1^2 + i\epsilon][k_2^2 + i\epsilon][(k - l)^2 + i\epsilon]} \\
&= 2\pi \delta(l^+ - p^+ - k^+ - q^+) \frac{1}{2z_1 l^+} \frac{1}{[z_2(1 - z_2)Q^2 + \mathbf{k}_1^2] \left[Q^2 + \frac{\mathbf{k}_1^2}{z_2} + \frac{\mathbf{k}_2^2}{z_3} + \frac{(\mathbf{k}_1 - \mathbf{k}_2)^2}{z_1} \right]} \\
I_{3,2} &= \int \frac{dk_1^+}{2\pi} \int \frac{dk_2^+}{2\pi} \int \frac{dk_1^-}{2\pi} \int \frac{dk_2^-}{2\pi} (2\pi)^3 \delta(p^+ - k_1^+ + k_2^+) \delta(k_1^+ - l^+ + q^+) \delta(k_2^+ - k^+) \\
&\quad \cdot \frac{1}{2k_1^+} \cdot \frac{(-2k^+)}{[(k_1 - k_2)^2 + i\epsilon][k_2^2 + i\epsilon][(k - l)^2 + i\epsilon]} \\
&= 2\pi \delta(l^+ - p^+ - k^+ - q^+) \frac{-1}{4z_1 z_2 (1 - z_2) \cdot (l^+)^2} \frac{1}{\left[Q^2 + \frac{\mathbf{k}_1^2}{z_2} + \frac{\mathbf{k}_2^2}{z_3} + \frac{(\mathbf{k}_1 - \mathbf{k}_2)^2}{z_1} \right]} \\
I_{4,i} &= I_{3,i}(\{p^+ \leftrightarrow q^+\}), \quad i = 1, 2. \tag{72}
\end{aligned}$$

If one wishes to evaluate Eq. (20) with gluon correlators in the target given in transverse momentum space, the above form of the integrals is already sufficient. If gluon correlators in the target are provided in transverse coordinate space, the corresponding Fourier transforms can be carried out using the integrals of appendix B of [19], which then allow to write our result in the large N_c limit in the form already presented in [1]. For completeness we present the large N_c result below⁵.

⁵Note that we corrected an error present in Eq. (12) of [1] as well as the a missing average factor for the transverse cross-section

3.7 The (large N_c) result

With α_{em} and α_s the electromagnetic and strong coupling constants, and e_f the electromagnetic charge of the quark with flavor f we obtain the following leading N_c result⁶:

$$\begin{aligned}
& \frac{d\sigma^{T,L}}{d^2\mathbf{p} d^2\mathbf{k} d^2\mathbf{q} dz_1 dz_2} = \\
& = c_{T,L} \cdot \frac{\alpha_s \alpha_{em} e_f^2 N_c^2}{z_1 z_2 z_3 \cdot 2} \prod_{i=1}^3 \prod_{j=1}^3 \int \frac{d^2\mathbf{x}_i}{(2\pi)^2} \int \frac{d^2\mathbf{x}'_j}{(2\pi)^2} e^{i\mathbf{p}(\mathbf{x}_1 - \mathbf{x}'_1) + i\mathbf{q}(\mathbf{x}_2 - \mathbf{x}'_2) + i\mathbf{k}(\mathbf{x}_3 - \mathbf{x}'_3)} \\
& \left\langle (2\pi)^4 \left[\left(\delta^{(2)}(\mathbf{x}_{13}) \delta^{(2)}(\mathbf{x}_{1'3'}) \sum_{h,g} \psi_{1;h,g}^{T,L}(\mathbf{x}_{12}) \psi_{1';h,g}^{T,L,*}(\mathbf{x}_{1'2'}) + \{1, 1'\} \leftrightarrow \{2, 2'\} \right) \right. \right. \\
& \quad \cdot N^{(4)}(\mathbf{x}_1, \mathbf{x}'_1, \mathbf{x}'_2, \mathbf{x}_2) + \left(\delta^{(2)}(\mathbf{x}_{23}) \delta^{(2)}(\mathbf{x}_{1'3'}) \sum_{h,g} \psi_{2;h,g}^{T,L}(\mathbf{x}_{12}) \psi_{1';h,g}^{T,L,*}(\mathbf{x}_{1'2'}) \right. \\
& \quad \left. \left. + \{1, 1'\} \leftrightarrow \{2, 2'\} \right) \cdot N^{(22)}(\mathbf{x}_1, \mathbf{x}'_1 | \mathbf{x}'_2, \mathbf{x}_2) \right] \\
& + (2\pi)^2 \left[\delta^{(2)}(\mathbf{x}_{13}) \sum_{h,g} \psi_{1;h,g}^{T,L}(\mathbf{x}_{12}) \psi_{3';h,g}^{T,L,*}(\mathbf{x}_{1'3'}, \mathbf{x}_{2'3'}) N^{(24)}(\mathbf{x}_{3'}, \mathbf{x}_{1'} | \mathbf{x}_{2'}, \mathbf{x}_2, \mathbf{x}_1, \mathbf{x}_{3'}) \right. \\
& \quad + \{1\} \leftrightarrow \{2\} + \delta^{(2)}(\mathbf{x}_{1'3'}) \sum_{h,g} \psi_{3;h,g}^{T,L}(\mathbf{x}_{13}, \mathbf{x}_{23}) \psi_{1';h,g}^{T,L,*}(\mathbf{x}_{1'2'}) \\
& \quad \left. \cdot N^{(24)}(\mathbf{x}_1, \mathbf{x}_3 | \mathbf{x}_{2'}, \mathbf{x}_2, \mathbf{x}_3, \mathbf{x}_{1'}) + \{1'\} \leftrightarrow \{2'\} \right] \\
& + \sum_{h,g} \psi_{3;h,g}^{T,L}(\mathbf{x}_{13}, \mathbf{x}_{23}) \psi_{3';h,g}^{T,L,*}(\mathbf{x}_{1'3'}, \mathbf{x}_{2'3'}) \cdot N^{(44)}(\mathbf{x}_1, \mathbf{x}_{1'}, \mathbf{x}_{3'}, \mathbf{x}_3 | \mathbf{x}_3, \mathbf{x}_{3'}, \mathbf{x}_{2'}, \mathbf{x}_2) \Big\rangle_{A^+}, \quad (73)
\end{aligned}$$

where $\psi_{i'} \equiv \psi_i$, $i = 1, \dots, 3$ and $z_3 = 1 - z_1 - z_2$, while $c_L = 1$, $c_T = 1/2$. To obtain sub-leading terms in N_c all operators $N^{(4)}, N^{(22)}, N^{(24)}, N^{(44)}$ are to be replaced by $1/N_c \cdot N^{(4)}(\mathbf{x}_1, \mathbf{x}_{1'}, \mathbf{x}_{2'}, \mathbf{x}_2)$. With ϕ_{ij} the azimuthal angle of \mathbf{x}_{ij} , $i, j = 1, \dots, 3$ and

$$X_j^2 = \mathbf{x}_{12}^2 (z_j + z_3) (1 - z_j - z_3), \quad j = 1, 2, \quad X_3^2 = z_1 z_2 \mathbf{x}_{12}^2 + z_1 z_3 \mathbf{x}_{13}^2 + z_2 z_3 \mathbf{x}_{23}^2, \quad (74)$$

we obtain

$$\begin{aligned}
\psi_{j,hg}^L &= -2\sqrt{2} Q K_0 (Q X_j) \cdot a_{j,hg}^{(L)}, & j = 1, 2 \\
\psi_{j,hg}^T &= 2ie^{\mp i\phi_{\mathbf{x}_{12}}} \sqrt{(1 - z_3 - z_j)(z_j + z_3)} Q K_1 (Q X_j) \cdot a_{j,hg}^{\pm}, & j = 1, 2 \\
\psi_{3,hg}^L &= 4\pi i Q \sqrt{2z_1 z_2} K_0 (Q X_3) (a_{3,hg}^{(L)} + a_{4,hg}^{(L)}), \\
\psi_{3,hg}^T &= -4\pi Q \sqrt{z_1 z_2} \frac{K_1 (Q X_3)}{X_3} (a_{3,hg}^{\pm} + a_{4,hg}^{\pm}). & (75)
\end{aligned}$$

With

$$a_{k+1,hg}^{T,L} = -a_{k,-hg}^{T,L}(\{p, \mathbf{x}_1\} \leftrightarrow \{q, \mathbf{x}_2\}), \quad k = 1, 2, \quad a_{j,hg}^{T,L} = a_{j,-hg}^{(-T,L)*}, \quad j = 1, \dots, 4. \quad (76)$$

⁶We note that the result presented below slightly differs from the result reported in the letter [1] where an erroneous overall factor of $1/(2\pi)^2$ has been included; we further corrected typos present in the expressions corresponding to Eq. (75) and Eq. (78) in [1].

we have for longitudinal photon polarizations

$$\begin{aligned}
a_{1,++}^{(L)} &= -\frac{(z_1 z_2)^{3/2} (z_1 + z_3)}{z_3 e^{-i\theta_p} |\mathbf{p}| - z_1 e^{-i\theta_k} |\mathbf{k}|}, & a_{1,-+}^{(L)} &= -\frac{\sqrt{z_1} z_2^{3/2} (z_1 + z_3)^2}{z_3 e^{-i\theta_p} |\mathbf{p}| - z_1 e^{-i\theta_k} |\mathbf{k}|}, \\
a_{3,++}^{(L)} &= \frac{z_1 z_2}{|\mathbf{x}_{13}| e^{-i\phi_{\mathbf{x}_{13}}}}, & a_{3,-+}^{(L)} &= \frac{z_2 (1 - z_2)}{|\mathbf{x}_{13}| e^{-i\phi_{\mathbf{x}_{13}}}},
\end{aligned} \tag{77}$$

while transverse polarization read

$$\begin{aligned}
a_{1,++}^{(+)} &= -\frac{(z_1 z_2)^{3/2}}{z_3 e^{-i\theta_p} |\mathbf{p}| - z_1 e^{-i\theta_k} |\mathbf{k}|}, \\
a_{1,-+}^{(+)} &= \frac{\sqrt{z_1} (z_2)^{3/2} (z_1 + z_3)}{z_1 e^{i\theta_k} |\mathbf{k}| - z_3 e^{i\theta_p} |\mathbf{p}|}, \\
a_{1,-+}^{(+)} &= \frac{\sqrt{z_1} z_2 (z_1 + z_3)^2}{z_3 e^{-i\theta_p} |\mathbf{p}| - z_1 e^{-i\theta_k} |\mathbf{k}|}, \\
a_{1,--}^{(+)} &= \frac{z_1^{3/2} \sqrt{z_2} (z_1 + z_3)}{z_3 e^{i\theta_p} |\mathbf{p}| - z_1 e^{i\theta_k} |\mathbf{k}|}, \\
a_{3,++}^{(+)} &= \frac{z_1 z_2 (z_2 z_3 |\mathbf{x}_{23}| e^{-i\phi_{\mathbf{x}_{23}}} + z_3 |\mathbf{x}_{13}| e^{-i\phi_{\mathbf{x}_{13}}} - z_1 z_2 |\mathbf{x}_{12}| e^{-i\phi_{\mathbf{x}_{12}}})}{(z_1 + z_3) |\mathbf{x}_{13}| e^{-i\phi_{\mathbf{x}_{13}}}}, \\
a_{3,+ -}^{(+)} &= \frac{z_2^2 (z_3 |\mathbf{x}_{23}| e^{-i\phi_{\mathbf{x}_{23}}} - z_1 |\mathbf{x}_{12}| e^{-i\phi_{\mathbf{x}_{12}}})}{|\mathbf{x}_{13}| e^{i\phi_{\mathbf{x}_{13}}}}, \\
a_{3,-+}^{(+)} &= -\frac{z_2 (z_1 + z_3) (z_3 |\mathbf{x}_{23}| e^{-i\phi_{\mathbf{x}_{23}}} - z_1 |\mathbf{x}_{12}| e^{-i\phi_{\mathbf{x}_{12}}})}{|\mathbf{x}_{13}| e^{-i\phi_{\mathbf{x}_{13}}}}, \\
a_{3,--}^{(+)} &= \frac{z_1 z_2 (z_1 |\mathbf{x}_{12}| e^{-i\phi_{\mathbf{x}_{12}}} - z_3 |\mathbf{x}_{23}| e^{-i\phi_{\mathbf{x}_{23}}})}{|\mathbf{x}_{13}| e^{i\phi_{\mathbf{x}_{13}}}}.
\end{aligned} \tag{78}$$

These expressions were already used to study azimuthal angular correlations between the three produced partons in DIS where it was shown that gluon saturation effects lead to a broadening and disappearance of the away side peaks. This is qualitatively similar to the disappearance of di-hadron angular correlations DIS [12] and in the forward rapidity region of high energy proton (deuteron)-nucleus collisions [9].

4 Summary

We have derived the triple differential cross section for production of a quark, anti-quark and a gluon in DIS for both transversely and longitudinally polarized photons. The final expression was already published in a short letter [1], here we show the full details of the calculation. After a discussion of the contributing diagrams in coordinate and momentum spaces, we give a brief overview of spinor helicity techniques and apply it to the process considered which leads to an enormous simplification of the Dirac Algebra involved. Besides being used for studying the effects of gluon saturation dynamics on azimuthal angular correlations of produced hadrons/jets in DIS, the resulting expressions can also be used, with trivial modification, to study three-jet production in ultra-peripheral heavy ion collisions at RHIC and the LHC using the CGC formalism. Furthermore, using the crossing symmetry of the

amplitudes one can relate this process to Multi Parton Interactions (MPI) in a proton at large x in processes where one produces a (real or virtual) photon and a jet (in case of DPI) or a (real or virtual) photon in case of TPI in the forward rapidity kinematics. If one assumes that the target is accurately described by the CGC formalism, one can then extract valuable information on intrinsic parton correlations at large x in a proton [26].

Acknowledgments

J.J-M. acknowledges support by the DOE Office of Nuclear Physics through Grant No. DE-FG02-09ER41620 and by the IDEX Paris-Saclay through a Jean d'Alembert grant and would like to thank L. Dixon for helpful correspondence on spinor helicity methods. Support has been received in part by UNAM-DGAPA-PAPIIT grant number IN101515 and by Consejo Nacional de Ciencia y Tecnología grant number 256494. M.H. acknowledges support by CONACyT-Mexico grant numbers CB-2014-22117 and Proy. No. 241408 as well as the Red-FAE. M.E.T.-Y. acknowledges support from CONACyT-México sabbatical grant number 232946 and the kind hospitality of ICN-UNAM provided in the initial stages of this collaboration.

References

- [1] A. Ayala, M. Hentschinski, J. Jalilian-Marian and M. E. Tejeda-Yeomans, Phys. Lett. B **761**, 229 (2016) doi:10.1016/j.physletb.2016.08.035 [arXiv:1604.08526 [hep-ph]].
- [2] F. Gelis, E. Iancu, J. Jalilian-Marian and R. Venugopalan, Ann. Rev. Nucl. Part. Sci. **60**, 463 (2010) doi:10.1146/annurev.nucl.010909.083629 [arXiv:1002.0333 [hep-ph]].
- [3] J. Jalilian-Marian, A. Kovner, L. D. McLerran and H. Weigert, Phys. Rev. D **55**, 5414 (1997); J. Jalilian-Marian, A. Kovner, A. Leonidov and H. Weigert, Nucl. Phys. B **504**, 415 (1997), Phys. Rev. D **59**, 014014 (1999), Phys. Rev. D **59**, 014015 (1999), Phys. Rev. D **59**, 034007 (1999), A. Kovner, J. G. Milhano and H. Weigert, Phys. Rev. D **62**, 114005 (2000); A. Kovner and J. G. Milhano, Phys. Rev. D **61**, 014012 (2000); E. Iancu, A. Leonidov and L. D. McLerran, Nucl. Phys. A **692**, 583 (2001), Phys. Lett. B **510**, 133 (2001); E. Ferreira, E. Iancu, A. Leonidov and L. McLerran, Nucl. Phys. A **703**, 489 (2002).
- [4] A. Dumitru and J. Jalilian-Marian, Phys. Rev. Lett. **89**, 022301 (2002) doi:10.1103/PhysRevLett.89.022301 [hep-ph/0204028]. A. Dumitru, A. Hayashigaki and J. Jalilian-Marian, Nucl. Phys. A **765**, 464 (2006) doi:10.1016/j.nuclphysa.2005.11.014 [hep-ph/0506308], Nucl. Phys. A **770**, 57 (2006) doi:10.1016/j.nuclphysa.2006.02.009 [hep-ph/0512129].
- [5] K. Akiba *et al.* [LHC Forward Physics Working Group Collaboration], J. Phys. G **43**, 110201 (2016) doi:10.1088/0954-3899/43/11/110201 [arXiv:1611.05079 [hep-ph]].
- [6] J. L. Albacete *et al.*, Int. J. Mod. Phys. E **25**, no. 9, 1630005 (2016) doi:10.1142/S0218301316300058 [arXiv:1605.09479 [hep-ph]].

- [7] D. Kharzeev, Y. V. Kovchegov and K. Tuchin, Phys. Rev. D **68**, 094013 (2003); J. L. Albacete, N. Armesto, A. Kovner, C. A. Salgado and U. A. Wiedemann, Phys. Rev. Lett. **92**, 082001 (2004); J. Jalilian-Marian, Y. Nara and R. Venugopalan, Phys. Lett. B **577**, 54 (2003) doi:10.1016/j.physletb.2003.09.097.
- [8] Z. B. Kang, I. Vitev and H. Xing, Phys. Rev. D **85**, 054024 (2012) doi:10.1103/PhysRevD.85.054024 [arXiv:1112.6021 [hep-ph]].
- [9] C. Marquet, Nucl. Phys. A **796**, 41 (2007).
- [10] A. Kovner and M. Lublinsky, JHEP **0611**, 083 (2006), Phys. Rev. D **84**, 094011 (2011), Phys. Rev. D **83**, 034017 (2011); J. Jalilian-Marian, Nucl. Phys. A **770**, 210 (2006); J. L. Albacete and C. Marquet, Phys. Rev. Lett. **105**, 162301 (2010).
- [11] J. Jalilian-Marian and Y. V. Kovchegov, Phys. Rev. D **70**, 114017 (2004) Erratum: [Phys. Rev. D **71**, 079901 (2005)] doi:10.1103/PhysRevD.71.079901, 10.1103/PhysRevD.70.114017 [hep-ph/0405266].
- [12] A. Accardi *et al.*, Eur. Phys. J. A **52**, no. 9, 268 (2016) doi:10.1140/epja/i2016-16268-9 [arXiv:1212.1701 [nucl-ex]]; L. Zheng, E. C. Aschenauer, J. H. Lee and B. W. Xiao, Phys. Rev. D **89**, no. 7, 074037 (2014) doi:10.1103/PhysRevD.89.074037 [arXiv:1403.2413 [hep-ph]].
- [13] B. B. Abelev *et al.* [ALICE Collaboration], Phys. Rev. Lett. **113**, no. 23, 232504 (2014) [arXiv:1406.7819 [nucl-ex]].
- [14] R. Aaij *et al.* [LHCb Collaboration], J. Phys. G **40**, 045001 (2013) [arXiv:1301.7084 [hep-ex]]; J. Phys. G **41**, 055002 (2014) [arXiv:1401.3288 [hep-ex]].
- [15] N. Armesto and A. H. Rezaeian, Phys. Rev. D **90**, no. 5, 054003 (2014) doi:10.1103/PhysRevD.90.054003 [arXiv:1402.4831 [hep-ph]]; V. P. Goncalves, B. D. Moreira and F. S. Navarra, Phys. Rev. C **90**, no. 1, 015203 (2014) doi:10.1103/PhysRevC.90.015203 [arXiv:1405.6977 [hep-ph]].
- [16] M. Hentschinski, A. Sabio Vera and C. Salas, Phys. Rev. Lett. **110** (2013) no.4, 041601 doi:10.1103/PhysRevLett.110.041601 [arXiv:1209.1353 [hep-ph]]; Phys. Rev. D **87**, no. 7, 076005 (2013) doi:10.1103/PhysRevD.87.076005 [arXiv:1301.5283 [hep-ph]]; I. Bautista, A. Fernandez Tellez and M. Hentschinski, Phys. Rev. D **94**, no. 5, 054002 (2016) doi:10.1103/PhysRevD.94.054002 [arXiv:1607.05203 [hep-ph]].
- [17] M. L. Mangano and S. J. Parke, Phys. Rept. **200**, 301 (1991); L. J. Dixon, In *Boulder 1995, QCD and beyond* 539-582 [hep-ph/9601359].
- [18] T. Lappi and R. Paatelainen, arXiv:1611.00497 [hep-ph].
- [19] G. Beuf, Phys. Rev. D **85**, 034039 (2012).
- [20] R. Boussarie, A. V. Grabovsky, L. Szymanowski and S. Wallon, JHEP **1611** (2016) 149 doi:10.1007/JHEP11(2016)149 [arXiv:1606.00419 [hep-ph]]; JHEP **1409** (2014) 026 doi:10.1007/JHEP09(2014)026 [arXiv:1405.7676 [hep-ph]].

- [21] I. Balitsky and G. A. Chirilli, Phys. Rev. D **83**, 031502 (2011) doi:10.1103/PhysRevD.83.031502 [arXiv:1009.4729 [hep-ph]]; Phys. Rev. D **87**, no. 1, 014013 (2013) doi:10.1103/PhysRevD.87.014013 [arXiv:1207.3844 [hep-ph]].
- [22] G. Beuf, Phys. Rev. D **94**, no. 5, 054016 (2016) doi:10.1103/PhysRevD.94.054016 [arXiv:1606.00777 [hep-ph]].
- [23] L. D. McLerran and R. Venugopalan, Phys. Rev. D **50**, 2225 (1994) doi:10.1103/PhysRevD.50.2225 [hep-ph/9402335]; A. J. Baltz, F. Gelis, L. D. McLerran and A. Peshier, Nucl. Phys. A **695**, 395 (2001) doi:10.1016/S0375-9474(01)01109-5 [nucl-th/0101024]; F. Gelis and A. Peshier, Nucl. Phys. A **697**, 879 (2002) doi:10.1016/S0375-9474(01)01264-7 [hep-ph/0107142]; I. I. Balitsky and A. V. Belitsky, Nucl. Phys. B **629**, 290 (2002) doi:10.1016/S0550-3213(02)00149-9 [hep-ph/0110158].
- [24] F. Gelis and J. Jalilian-Marian, Phys. Rev. D **67**, 074019 (2003) doi:10.1103/PhysRevD.67.074019 [hep-ph/0211363].
- [25] C. Cruz-Santiago, P. Kotko and A. M. Staśto, Prog. Part. Nucl. Phys. **85**, 82 (2015). doi:10.1016/j.pnpnp.2015.07.002 A. van Hameren, P. Kotko and K. Kutak, JHEP **1301**, 078 (2013) doi:10.1007/JHEP01(2013)078 [arXiv:1211.0961 [hep-ph]].
- [26] A. Kovner and A. H. Rezaeian, arXiv:1701.00494 [hep-ph].